Commun Nonlinear Sci Numer Simulat 44 (2017) 52–73

Contents lists available at ScienceDirect

Commun Nonlinear Sci Numer Simulat

journal homepage: www.elsevier.com/locate/cnsns

Research paper

Hopf and steady state bifurcation analysis in a ratio-dependent predator–prey model

Lai Zhang[a], Jia Liu[b], Malay Banerjee[c,*]

[a] Department of Mathematics and Mathematical Statistics, Umeå University, SE-90187, Umeå, Sweden
[b] School of Mathematics and Physics, Changzhou University, Changzhou 213164, China
[c] Department of Mathematics and Statistics, Indian Institute of Technology, Kanpur-208016, India

ARTICLE INFO

Article history:
Received 25 March 2016
Revised 23 July 2016
Accepted 25 July 2016
Available online 29 July 2016

Keywords:
Prey–predator model
Turing instability
Pattern formation
Spatiotemporal bifurcation
Non-constant steady state

ABSTRACT

In this paper, we perform spatiotemporal bifurcation analysis in a ratio-dependent predator–prey model and derive explicit conditions for the existence of non-constant steady states that emerge through steady state bifurcation from related constant steady states. These explicit conditions are numerically verified in details and further compared to those conditions ensuring Turing instability. We find that (1) Turing domain is identical to the parametric domain where there exists only steady state bifurcation, which implies that Turing patterns are stable non-constant steady states, but the opposite is not necessarily true; (2) In non-Turing domain, steady state bifurcation and Hopf bifurcation act in concert to determine the emergent spatial patterns, that is, non-constant steady state emerges through steady state bifurcation but it may be unstable if the destabilising effect of Hopf bifurcation counteracts the stabilising effect of diffusion, leading to non-stationary spatial patterns; (3) Coupling diffusion into an ODE model can significantly enrich population dynamics by inducing alternative non-constant steady states (four different states are observed, two stable and two unstable), in particular when diffusion interacts with different types of bifurcation; (4) Diffusion can promote species coexistence by saving species which otherwise goes to extinction in the absence of diffusion.

1. Introduction

A characteristic feature of ecological systems is the complex interactions among individuals and the interactions between individuals and their surrounding environment [25], which occur over a wide range of spatial and temporal scales. The spatial component has been identified as an important factor in determining the distribution of populations with the advancement of time and the structure of communities over their habitats. Experimental evidence suggests that movement rates of interacting individuals can dramatically affect population stability [12,20] and the composition of communities [8,21]. A consequence of individual movement behaviour is the spatial heterogeneity of individual abundance within the ecosystem which is observable at the macroscopic levels of population and community. Spatial pattern is a ubiquitous scenario in nature and often takes the role of modifying the temporal dynamics and regulating population stability [23,37]. In recent decades, a significant body of literature has explored the interactions between individual movement behaviours and spatial

* Corresponding author. Fax: +91 512 259 7500.
E-mail address: malayb@iitk.ac.in (M. Banerjee).

http://dx.doi.org/10.1016/j.cnsns.2016.07.027
1007-5704/

patterns with the ultimate goal of understanding how spatial component influences the dynamics of populations and the structure of communities.

A convenient approach to describe the spatiotemporal population dynamics is the reaction-diffusion framework [29], which is a way of relating dynamics at the individual level to the dynamics at the population level. In spite of its simple representation, reaction-diffusion systems can generate a wide variety of spatial patterns, giving this framework a powerful potential for application as an experimental hypothesis in a wide variety of biological phenomena [14]. Reaction-diffusion systems were first used to explain the formation of spatial patterns in ecological systems by Segel and Jackson [35], inspired by the seminal work of Turing [45]. Since then, numerous studies under the reaction-diffusion framework have been devoted to the description of spatial patterns [13,22], to the identification of its drivers [5,6,15,32,52], and to the implications for community dynamics [10,26,27,34]. Many important and interesting findings have been unrevealed. For instance, the author in [13] simulated both regular and irregular patterns in semiarid vegetation using reaction-diffusion system and found that the theoretically predicted patterns are in close agreement with field observations. Baurmann et al. [6] investigated different instability mechanisms behind the emergence of spatial patterns in an ecological prey–predator system.

Turing instability and Turing–Hopf bifurcation are two well known mechanisms behind the formation of spatial pattern [5,6,41]. The concept of Turing instability is that the locally stable homogeneous steady state becomes unstable due to small amplitude heterogeneous perturbation around the homogeneous steady states, leading to the formation of spatially heterogeneous distribution of population over their habitats [35,45]. The emergent spatial patterns due to Turing instability are stationary [3,9,48], which are also known as Turing patterns such as spots, strips or mixture of spots and strips. The basic idea of the Turing–Hopf bifurcation is that the locally unstable homogeneous steady state evolves into non-stationary spatial patterns under spatially inhomogeneous spatial perturbation. Non-stationary spatial patterns are characterized by periodic, qausi-periodic or even chaotic patterns as time advances. Besides these two mechanisms, other mechanisms such as biological invasion, turbulence, travelling wave, periodic travelling wave can also be responsible for spatial pattern formation [23,38,42,46].

The spatial patterns generated by the aforementioned two mechanisms can be obtained by numerical simulations, and the conditions for Turing and Hopf bifurcations can be reached by means of local stability analysis around the suitable homogeneous steady state [6,48]. These techniques can predict the regions in the targeted parametric space where we can observe spatial patterns but they are unable to predict the spatial patterns generated by large amplitude spatiotemporal perturbations. Non-constant steady states have been suggested as a fundamental argument for the existence of spatial patterns, and received great attention from various researchers [18,30,31,39,40,50]. However, the complexity of the (generally implicit) conditions for the existence of non-constant steady states makes it very hard to verify them numerically. Thus, the relationship between the emergent spatial patterns including Turing patterns and the non-constant steady states remains poorly understood. Undoubtably, clear clarification of this relationship is of paramount importance in comprehensive understanding of spatiotemporal dynamics and spatial pattern formation as it bridges numerical results on emergent spatial patterns and theoretical predictions of non-constant steady states [4]. This paper is devoted to the clarification of this intimate relationship. To this aim, we consider a spatiotemporal prey–predator model with a ratio-dependent functional response in one dimensional spatial domain in order to derive precise and explicit conditions for the existence of non-constant steady state within the parametric restrictions that are satisfied for the stability and instability of constant steady state, an important and interesting aspect that has been overlooked by most of the researchers.

Predator–prey models with ratio-dependent functional response for predator consumption are widely implemented in ecological modelling and the ratio-dependent functional response has been strongly supported by numerous field and laboratory experiments [2,7,11,33]. A great number of theoretical works aim for understanding the formation of spatial patterns in ratio-dependent diffusive predator–prey models by means of the standard Turing–Hopf bifurcation analysis (e.g., [1,36,49]), the norm form and centre manifold theory for determining the direction and stability of Hopf bifurcation (e.g., [43,53]), and the technique of steady-state bifurcation (e.g., [4,47]). The former two approaches consider spatiotemporal dynamic models to derive the conditions under which purely spatially or temporarily periodic pattern occurs, while the last approach attempts to establish a link between the spatial patterns observed in the spatiotemporal models with the spatially heterogeneous steady state of the associated elliptic systems. The current paper combines the first and last approach by numerically comparing the parametric restrictions that are satisfied for existence of non-constant steady state and the conditions that are satisfied for Turing instability.

The paper is organised as follows. In the next section, we describe the temporal model and recall its basic dynamical features to understand the local stability of constant steady states with the help of complete global bifurcation analysis. In Section 3, we introduce the spatiotemporal model and present Turing instability results. Special attention is paid to the emergent stationary and non-stationary spatial patterns. Then we derive the general conditions in Section 4 ($\Omega \subset R^n$) and more explicit conditions in Section 5 ($\Omega \subset R$) for the existence of non-constant steady states in order to facilitate numerical analysis which is carried out in the coming section. In Section 6 we carry out detailed numerical simulations to verify the analytical findings obtained in Section 5 and most importantly cross verify the existence conditions of non-constant steady states and compare them to those conditions of Turing as well as Turing–Hopf bifurcations. The paper is closed with a conclusion section. The reason for Section 4 is to keep the completeness and generality of this paper and that part of the conclusions in that section will be referred to later in Section 5. However, readers who are interested in numerical analysis can skip Section 4 without causing any confusion.

2. Temporal model

The temporal model for the ratio-dependent prey–predator interaction with modified Holling–Tanner formalism is governed by the following system of coupled nonlinear ordinary differential equations

$$\frac{du}{dt} = u\left(\alpha_1 - \beta_1 u - \frac{\gamma_1 v}{m_1 v + u}\right), \tag{2.1}$$

$$\frac{dv}{dt} = v\left(\alpha_2 - \frac{\gamma_2 v}{m_2 + u}\right) \tag{2.2}$$

with a positive initial condition $(u(0), v(0)) > 0$. The population biomass of prey and predator at time t are denoted by $u(t)$ and $v(t)$. All parameters α_1, β_1, γ_1, m_1, α_2, γ_2, m_2 are positive. α_1 and α_2 are the intrinsic growth rates of prey and predator. The positive α_2 means that predator has extra food source and can survive even if the prey goes to extinction. Hence the predator is a generalist. β_1 is the intra-specific competition rate of prey and α_1/β_1 stands for the environmental carrying capacity of the prey. Predation rate on prey follows the Michaelis–Menten–Holling type functional response, which is characterized by γ_1 and m_1. γ_1 is the rate of capture of prey by the predator and m_1 is a dimensionless quantity and inversely proportional to the handling time. γ_2 is the strength of intra-species competition for the predator and m_2 is the measure of the environmental carrying capacity for the predator when the most favourable food source is absent. In other words, m_2 measures the extent up to which the environment can support the growth of the predator when $u(t) = 0$.

The prey–predator model described by the system of (2.1) and (2.2) is known as modified Holling–Tanner model with a ratio-dependent functional response [24]. The word "modified" stands for two consecutive modifications of the original Holling–Tanner model [44]. Liang and Pan [16] first modified the original Holling–Tanner model by replacing the Holling type-II functional response with the ratio-dependent functional response. It is important to mention here that the model proposed and analysed by Liang and Pan was mentioned as a ratio-dependent Holling–Tanner model in their work. The phrase "modified Holling–Tanner model" was first used by Nindjin et al. [28] where the authors first introduced the constant term m_2 into the predator growth equation. Combining these two modifications into a single model, Mandal and Banerjee [24] studied the complete dynamics of the model (2.1) and (2.2) within deterministic as well as stochastic environment. The Holling–Tanner model was first proposed and analysed with the assumption that some predator species can survive when the concentration of their most favourable food source is very low as they can survive on alternative food source also. That is why such kind of predators are known as generalist. In some situations it is quite natural to consider the ratio-dependent functional response to describe the grazing of prey by their predators so it is important to study the dynamics of a prey–predator model involving generalist predator but the grazing law follows the ratio-dependent functional response. This results in the analysis carried out by Liang and Pan [16]. The classical Holling–Tanner model and Holling–Tanner model with ratio-dependent functional response fail to satisfy the continuity condition when both the populations approach zero. To overcome this mathematical difficulty and in order to take care of prey independent carrying capacity for the predator population, the modified Holling–Tanner model came into the picture. Now this modification is well accepted due to the validation of the model from mathematical viewpoint as well as it is able to capture several realistic features of prey–predator interaction with generalist predator.

The dynamical behaviour of the temporal model has been discussed in detail by [24]. For the completeness we briefly summarize the existence and local asymptotic stability conditions for coexisting steady states which are relevant to the forthcoming discussion of our present work. By direct calculation, we note that the positive constant steady states of the model (2.1) and (2.2) are the points of intersection(s) of the curve $\alpha_1 - \beta_1 u - \frac{\gamma_1 v}{u + m_1 v} = 0$ and the straight line $\gamma_2 v = \alpha_2(u + m_2)$ in the interior of first quadrant. The conditions for the existence of positive steady states can be divided into three cases.

Case A: $\alpha_1 m_1 = \gamma_1$ and $\alpha_1\gamma_2 > \beta_1 m_1 \alpha_2 m_2$.

The model (2.1) and (2.2) has a unique positive steady state $E_0^* = (\hat{u}_0, \hat{v}_0)$, where

$$\hat{u}_0 = \frac{\alpha_1\gamma_2 - \beta_1 m_1 \alpha_2 m_2}{\beta_1 m_1 \alpha_2 + \beta_1\gamma_2}, \quad \hat{v}_0 = \frac{\alpha_2(m_2 + \hat{u}_0)}{\gamma_2}.$$

Case B: $\alpha_1 m_1 > \gamma_1$.

The model (2.1) and (2.2) has a unique positive steady state $E_1^* = (\hat{u}_1, \hat{v}_1)$, where

$$\hat{u}_1 = \frac{-b + \sqrt{b^2 - 4ac}}{2a}, \quad \hat{v}_1 = \frac{\alpha_2(m_2 + \hat{u}_1)}{\gamma_2}, \tag{2.3}$$

and

$$a = \beta_1(m_1\alpha_2 + \gamma_2),$$
$$b = \beta_1 m_1 \alpha_2 m_2 + \alpha_2(\gamma_1 - \alpha_1 m_1) - \alpha_1\gamma_2,$$
$$c = \alpha_2 m_2(\gamma_1 - \alpha_1 m_1).$$

Case C: $\alpha_1 m_1 < \gamma_1$ and $b < 0, b^2 \geq 4ac$. (2.4)

The model (2.1) and (2.2) has two positive steady states $E_2^* = (\hat{u}_2, \hat{v}_2)$ and $E_3^* = (\hat{u}_3, \hat{v}_3)$ where

$$\hat{u}_2 = \frac{-b - \sqrt{b^2 - 4ac}}{2a}, \ \hat{u}_3 = \frac{-b + \sqrt{b^2 - 4ac}}{2a}, \ \hat{v}_i = \frac{\alpha_2(m_2 + \hat{u}_i)}{\gamma_2}, \ i = 2, 3. \tag{2.5}$$

E_0^* and E_1^* are locally asymptotically stable whenever they are feasible. We find two interior equilibrium points E_2^* and E_3^* when the parametric restriction mentioned in Case C is satisfied. Among these two equilibria, E_2^* is always a saddle point and E_3^* is locally asymptotically stable if $a_{11} + a_{22} < 0$, where

$$a_{11} = \left.\frac{\partial F_1(u,v)}{\partial u}\right|_{(u,v)=(\hat{u}_3,\hat{v}_3)}, \quad a_{22} = \left.\frac{\partial F_2(u,v)}{\partial u}\right|_{(u,v)=(\hat{u}_3,\hat{v}_3)},$$

and $F_1 = u(\alpha_1 - \beta_1 u - \frac{\gamma_1 v}{u + m_1 v})$, $F_2 = v(\alpha_2 - \frac{\gamma_2 v}{u + m_2})$. Only the stability property of E_3^* can be altered as it loses stability through Hopf bifurcation. Two interior equilibrium points E_2^* and E_3^* can collide and disappear through saddle-node bifurcation. The parametric conditions for the Hopf and saddle-node bifurcations can be written implicitly as $a_{11} + a_{22} = 0$ and $b^2 = 4ac$.

To understand the change in dynamic behaviour with the variation in model parameters, we now consider a numerical example. For this purpose we fix the parameter values $\alpha_1 = 2$, $\beta_1 = 0.8$, $m_1 = 0.2$, $\gamma_2 = 0.45$, $m_2 = 0.1$ and consider γ_1, α_2 as bifurcation parameters. In Fig. 1(a) we have presented the bifurcation diagram. Vertical dashed line represents the curve $\gamma_1 = \alpha_1 m_1$, and on the left region of this line (region R_1) we find a unique interior equilibrium point which is globally asymptotically stable (see Fig. 1(b)). On the right hand side of the vertical dashed line we have either two interior equilibrium points, when parameter values belong to the domain $R_2 \cup R_3 \cup R_4$, or no equilibrium point for $(\gamma_1, \alpha_2) \in R_5$. Black curve represents the saddle-node bifurcation curve on which two interior equilibrium points collide. On the saddle-node bifurcation curve we find Bogdanov–Takens bifurcation point (denoted by a magenta coloured point) from which one local and one global bifurcation curve emerge. The orange curve is the Hopf bifurcation curve and cyan coloured curve is the Homoclinic bifurcation curve. For parameter values lying in domain R_2, we find a stable interior equilibrium point (E_3^*) and a saddle interior equilibrium (E_2^*) where the stable manifold of E_2^* is the boundary for the basin of attraction of E_3^* (see Fig. 1(c)). We find locally stable interior equilibrium point E_3^* surrounded by an unstable limit cycle for parameters lying in R_3 and a sample phase portrait is presented in Fig. 1(d). Interior equilibrium point E_3^* loses stability through Hopf bifurcation when we enter the parametric domain R_4 and we find an unstable focus E_3^* and a saddle point E_2^* (see Fig. 1(e)). For parameter values in domain R_5, we can see that prey population goes to extinction but predator can survive at the carrying capacity.

3. Spatiotemporal model

Now and onwards, we consider the spatiotemporal dynamics produced by the ratio-dependent prey–predator model coupled with self-diffusion, which is described by the following partial differential equations

$$\frac{\partial u}{\partial t} = u\left(\alpha_1 - \beta_1 u - \frac{\gamma_1 v}{m_1 v + u}\right) + \Delta u, \tag{3.1}$$

$$\frac{\partial v}{\partial t} = v\left(\alpha_2 - \frac{\gamma_2 v}{m_2 + u}\right) + d\Delta v, \tag{3.2}$$

for $(X, t) \in \Omega \times R^+$, and subject to a non-negative initial condition

$$u(X, 0) = u_0(X) \geq 0, v(X, 0) = v_0(X) \geq 0, X \in \Omega,$$

and non-flux boundary condition

$$\frac{\partial u}{\partial \nu} = \frac{\partial v}{\partial \nu} = 0, X \in \partial\Omega, t > 0. \tag{3.3}$$

The positive parameter d in equation (3.2) stands for the rate of diffusion of the predator and we have assumed the rate of diffusion for the prey species is equal to one. $\Delta \equiv (\partial^2/\partial x^2) + (\partial^2/\partial y^2)$ is a two dimensional Laplacian operator in variable $X \equiv (x, y) \in \Omega \subset R^2$ and Ω is a square bounded domain whose boundary is denoted by $\partial\Omega$. $\partial/\partial\nu$ indicates the outward drawn normal derivative on the boundary $\partial\Omega$.

One can easily verify that any constant equilibrium solution to the temporal model (2.1) and (2.2) is a spatially homogeneous steady state for the spatiotemporal model (3.1) and (3.2). Now we seek for conditions for occurrence of Turing instability which leads to emergence of spatially inhomogeneous steady state that results from the small amplitude heterogeneous perturbation around a stable positive homogeneous steady state. In previous section, we show that E_1^* is locally stable, E_2^* is always a saddle-point, and E_3^* can be locally stable depending on the specific parametric restriction. Hence we only consider E_1^* and E_3^* for Turing instability. In fact, standard Turing analysis shows that there is no Turing instability occurring around E_1^* (Appendix A). In the rest of this section we only consider spatial patterns with respect to E_3^*.

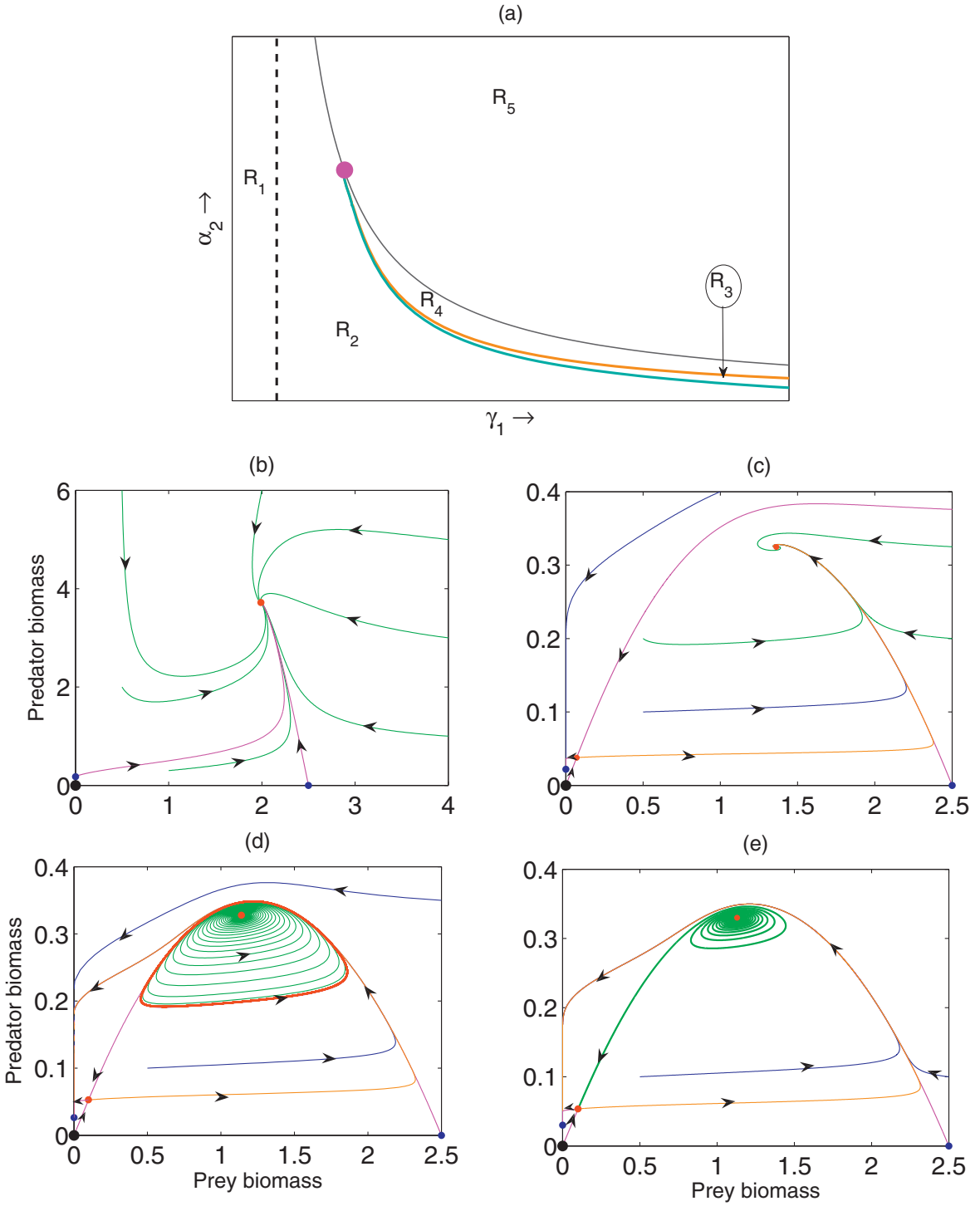

Fig. 1. (a) Two dimensional schematic bifurcation diagram for the model (2.1) and (2.2) in $\gamma_1 - \alpha_2$−parametric space. Interpretation of curves and regions of R_1 to R_5 can be found in the main text. Sample phase portraits for the choice of parameter values from domain R_1 to R_4 keeping $\alpha_1 = 2$, $\beta_1 = 0.8$, $m_1 = 0.2$, $\gamma_2 = 0.45$, $m_2 = 0.1$ fixed. (b) $(\gamma_1, \alpha_2) = (0.3, 0.8) \in R_1$, (c) $(\gamma_1, \alpha_2) = (4, 0.1) \in R_2$, (d) $(\gamma_1, \alpha_2) = (4, 0.11906) \in R_3$, (e) $(\gamma_1, \alpha_2) = (4, 0.12) \in R_4$.

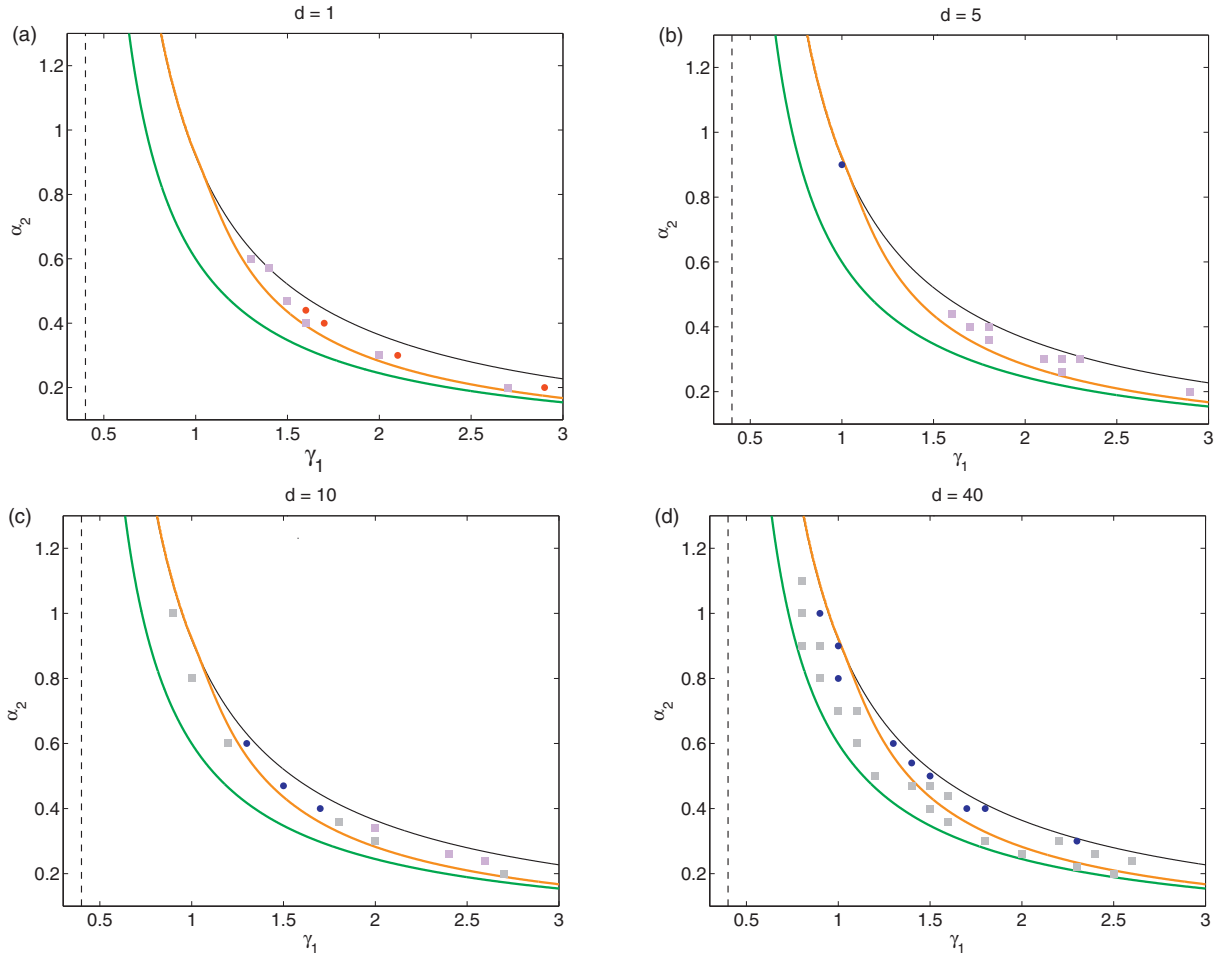

Fig. 2. Pattern diagram in the $\gamma_1 - \alpha_2-$ parameter space for different diffusion ratio d. Grey squares (■) symbolise the stationary spot patterns and blue cycles (●) the stationary patterns of mixed spot and strip. Purple squares (■) symbolise dynamical chaotic patterns while red cycles (●) dynamical spiral patterns. The region surrounded by the green and orange curves is the Turing domain where Turing instability occurs at E_3^*. The four types of observed patterns are illustrated in Fig. 3. Interpretation of other curves can be found in Fig. 1a. Parameter values are $\alpha_1 = 2$, $\beta_1 = 0.8$, $\gamma_1 = 1.4$, $\gamma_2 = 0.45$, $m_1 = 0.2$, $m_2 = 0.1$. (For interpretation of the references to colour in this figure legend, the reader is referred to the web version of this article.)

We now illustrate the Turing bifurcation around E_3^* and spatial patterns generated by spatiotemporal model (3.1) and (3.2) through numerical simulations. Numerical simulations are performed over a 200 × 200 lattice with a space-step $\delta x = \delta y = 1$ and a time-step δt satisfying

$$d\delta t\left(\frac{1}{(\delta x)^2} + \frac{1}{(\delta y)^2}\right) < 0.5. \tag{3.4}$$

The reported patterns are independent of the choice of the space and time steps as long as the condition (3.4) is valid. All numerical simulations are carried out using the forward Euler scheme for the temporal part and five point finite difference scheme for the diffusion part. Population biomass of prey and predator that are sitting at spatially homogeneous steady state is perturbed with a small amplitude heterogeneous random Gaussian noise which is spatially uncorrelated [5].

Fig. 2 summarises the Turing bifurcation curve and distribution of emergent spatial patterns in the parameter space spanned by γ_1 and α_2. Note that each point in this parameter space represents a whole class of system. Apparently, stationary spatial patterns are found in both Turing domain where E_3^* is locally stable but Turing unstable and Hopf domain where E_3^* is locally unstable, while non-stationary patterns are found only in the Hopf domain. In addition the non-stationary pattern in general arises with small diffusion rate. With an increase in diffusion rate, these dynamical patterns are replaced by stationary patterns. In total we observe four types of spatial patterns: spots, mixture of spot and strip, spirals, and chaos (see Fig. 3). The former two are stationary in time while the other two are non-stationary in nature.

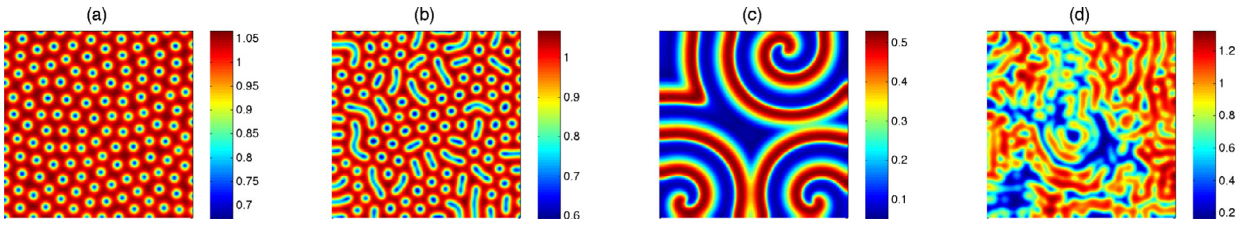

Fig. 3. Samples of four different types of spatial patterns (a) cold spot, (b) mixture of spot and strip, (3) spiral pattern, and (d) chaos. Parameter values are $\alpha_1 = 2,\ \beta_1 = 0.8,\ \gamma_1 = 1.4,\ \gamma_2 = 0.45,\ m_1 = 0.2,\ m_2 = 0.1,$ and $\alpha_2 = 0.47, d = 20$ (a) $\alpha_2 = 0.54, d = 20$ (b), $\alpha_2 = 0.2, \gamma_1 = 2.9, d = 1$ (c), and $\alpha_2 = 0.57, d = 5$ (d).

4. Spatiotemporal bifurcations ($\Omega \subset R^n$)

In this section we analytically derive the condition for the existence of non-constant steady state using the approach presented in [31]. To this end we consider the following elliptic system corresponding to the system (3.1) and (3.2)

$$-\Delta u = u\left(\alpha_1 - \beta_1 u - \frac{\gamma_1 v}{m_1 v + u}\right), \tag{4.1}$$

$$-d\Delta v = v\left(\alpha_2 - \frac{\gamma_2 v}{m_2 + u}\right), \tag{4.2}$$

under the non-flux boundary condition (3.3). Solutions of the system (4.1) and (4.2) are steady states of the system (3.1) and (3.2). Clearly any constant solutions of the system (4.1) and (4.2) are also steady state to the system (3.1) and (3.2). Here we are interested in the non-constant steady states. However, the stability of the constant steady state of the system (3.1) and (3.2) is intimately related to the existence of non-constant solution of the elliptic system (4.1) and (4.2). In fact, the instability of a constant steady state may give rise to either periodic solution through Hopf bifurcation or non-constant steady state through steady state bifurcation. This is the strategy we adopt in this section to seek for conditions for the existence of non-constant steady states.

Here and onwards we will be considering the systems (3.1) and (3.2) and (4.1) and (4.2) for $X \equiv x \in \Omega \subset R^n$. For notational convenience, we denote the constants $\alpha_1, \alpha_2, \beta_1, \gamma_1, \gamma_2, m_1, m_2$ collectively by Λ and

$$\theta_i = \frac{\gamma_1 \hat{u}_i \hat{v}_i}{(m_1 \hat{v}_i + \hat{u}_i)^2} - \beta_1 \hat{u}_i, \quad \delta_i = \frac{\gamma_1 (\hat{u}_i)^2}{(m_1 \hat{v}_i + \hat{u}_i)^2}, \quad g_i = \delta_j \alpha_2^2/\gamma_2 - \alpha_2 \theta_i. \tag{4.3}$$

The formulas in (4.3) will be referred to frequently in the rest of this paper. We also give a priori estimate for the positive upper and lower bounds for the positive solutions of system (4.1) and (4.2) in Theorem 4.1, which will be recalled later. The proof of this theorem follows the standard theory of partial differential equations and is deferred to Appendix B.

Theorem 4.1. *Let $\alpha_1 m_1 \neq \gamma_1$. There exist positive constants $\underline{C}$ and $\overline{C}$ depending on Λ and Ω such that any positive solution $(u(x), v(x))$ of the system (4.1) and (4.2) satisfies*

$$\underline{C} < u, v < \overline{C}.$$

From now on, we always let parameters $\alpha_1, \alpha_2, \beta_1, \gamma_1, \gamma_2, m_1, m_2$ be fixed and consider the diffusion coefficient d as the bifurcating parameter. We consider two cases: $\alpha_1 m_1 > \gamma_1$ and $\alpha_1 m_1 < \gamma_1$. The former condition ensures that the system (3.1) and (3.2) has a unique constant steady state $E_1^* = (\hat{u}_1, \hat{v}_1)$ (see equations in (2.3)). The Theorem 4.2 below proves that this constant steady state is locally asymptotically stable. In the latter case (i.e., $\alpha_1 m_1 < \gamma_1$), we further assume the following condition is satisfied to ensure the existence of the two different constant steady states $E_2^* = (\hat{u}_2, \hat{v}_2)$ and $E_3^* = (\hat{u}_3, \hat{v}_3)$ (see equations in (2.5)),

$$[\alpha_2(\gamma_1 - \alpha_1 m_1) + \beta m_1 m_2 \alpha_2 - \alpha_1 \gamma_2]^2 > 4\alpha_2 \beta_1 m_2 (\gamma_1 - \alpha_1 m_1)(\gamma_2 + \alpha_2 m_1), \tag{4.4}$$

which is actually the condition (2.4) excluding the special case of $E_2^* = E_3^*$. There are three situations to be considered: (1) $u^* > \hat{u}_3$, (2) $\hat{u}_2 < u^* < \hat{u}_3$, (3) $u^* < \hat{u}_2$, where

$$u^* = \frac{\alpha_1 m_1 - \gamma_1 + \sqrt{\gamma_1(\gamma_1 - \alpha_1 m_1)}}{m_1 \beta_1}. \tag{4.5}$$

These three situations are addressed sequentially in Theorems 4.3–4.5.

For simplicity, we introduce a notation $\mathbf{w} = (u, v)$ and set

$$D = \begin{pmatrix} 1 & 0 \\ 0 & d \end{pmatrix}, \quad G(\mathbf{w}) = \begin{pmatrix} u\left(\alpha_1 - \beta_1 u - \dfrac{\gamma_1 v}{m_1 v + u}\right) \\ v\left(\alpha_2 - \dfrac{\gamma_2 v}{m_2 + u}\right) \end{pmatrix}, \quad G_{\mathbf{w}}(E_i^*) = \begin{pmatrix} \theta_i & -\delta_i \\ \alpha_2^2/\gamma_2 & -\alpha_2 \end{pmatrix},$$

where θ_i and δ_i can be found in (4.3).

Let $0 = \mu_0 < \mu_1 < \mu_2 < \cdots$ be all the eigenvalues of the operator $-\Delta$ on Ω with the homogeneous Neumann boundary condition. These eigenvalues have explicit expressions in case of one dimensional spatial domain (see Section 5). Set $\mathbf{X} = \{\mathbf{w} \in [C^1(\bar{\Omega})]^2 \mid \partial_\gamma \mathbf{w} = 0, x \in \partial\Omega\}$, $\mathbf{X}^+ = \{\mathbf{w} \in [C^1(\bar{\Omega})]^2 \mid \mathbf{w} > 0, x \in \bar{\Omega}\}$, and let X_j be the eigenspace corresponding to μ_j in $C^1(\bar{\Omega})$, and $\{\phi_{jl} : l = 1, \cdots, n(\mu_j)\}$ be an orthogonal basis of $\mathbf{X}_j$, and $\mathbf{X}_{jl} = \{\mathbf{c}\phi_{jl} \mid \mathbf{c} \in \mathbb{R}^2\}$. Here, $n(\mu_j)$ is the multiplicity of μ_j. Then,

$$\mathbf{X} = \bigoplus_{j=1}^{\infty} \mathbf{X}_j, \quad \mathbf{X}_j = \bigoplus_{l=1}^{n(\mu_j)} \mathbf{X}_{jl}.$$

Moreover, the system (4.1) and (4.2) can be written as

$$-\Delta \mathbf{w} = D^{-1} G(\mathbf{w}). \tag{4.6}$$

Applying the fixed point index method, we see that finding positive solutions of the problem (4.6) is equivalent to find positive solutions of the equation

$$f(d; \mathbf{w}) =: \mathbf{w} - (\mathbf{I} - \Delta)^{-1}\{D^{-1} G(\mathbf{w}) + \mathbf{w}\} \quad \text{on } \mathbf{X},$$

where $(\mathbf{I} - \Delta)^{-1}$ is the inverse of $\mathbf{I} - \Delta$ with the homogeneous Neumann boundary condition. A direct computation shows that

$$D_{\mathbf{w}} f(d; E_i^*) = \mathbf{I} - (\mathbf{I} - \Delta)^{-1}(D^{-1} G_{\mathbf{w}}(E_i^*) + \mathbf{I}). \tag{4.7}$$

By the Leray–Schauder Theorem, we have that if $D_{\mathbf{w}} f(d; E_i^*)$ is invertible, then

$$\text{index}(f(d; \cdot), E_i^*) = (-1)^r \quad \text{with} \quad r = \sum_{\xi < 0} n_\xi,$$

where n_ξ is the algebraic multiplicity of the negative eigenvalue ξ of (4.7).

By means of (4.6), we get that for each $\mathbf{X}_j$, ξ is an eigenvalue of (4.7) on $\mathbf{X}_j$ if and only if $\xi(1 + \mu_j)$ is an eigenvalue of the matrix

$$\mu_j \mathbf{I} - D^{-1} G_{\mathbf{w}}(E_i^*) = \begin{pmatrix} \mu_j - \theta_i & \delta_i \\ -d^{-1}\alpha_2^2/\gamma_2 & \mu_j + d^{-1}\alpha_2 \end{pmatrix}.$$

Write

$$H_i(d; \mu) =: d \det(\mu \mathbf{I} - D^{-1} G_{\mathbf{w}}(\hat{\mathbf{w}})) = d\mu^2 + \mu(\alpha_2 - d\theta_i) + g_i,$$

where g_i can be found in (4.3). Thus, $D_{\mathbf{w}} f(d; E_i^*)$ is invertible if and only if $H_i(d; \mu_j) \neq 0$ for $j \geq 0$. Moreover, the number of negative eigenvalues of $D_{\mathbf{w}} f(d; E_i^*)$ on $\mathbf{X}_{jl}$ is odd if and only if $H_i(d; \mu_j) < 0$. Hence, we have the following proposition.

Proposition 4.1. *Suppose that $H_i(d; \mu_j) \neq 0$ for all $j \geq 0$. Then*

$$\text{index}(f(d; \cdot), E_i^*) = (-1)^\sigma, \quad \sigma = \sum_{j \geq 0, H_i(d; \mu_j) < 0} n(\mu_j),$$

where $n(\mu_j)$ is the multiplicity of μ_j.

From Proposition 4.1, in order to calculate the index of $f(d; \cdot)$ at E_i^*, we only consider the sign of $H_i(d; \mu_j)$. If

$$(\alpha_2 - d\theta_i)^2 > 4dg_i, \tag{4.8}$$

then $H_i(d; \mu) = 0$ has two real roots, namely,

$$\mu_+^{(i)}(d) = (\theta_i d - \alpha_2 + \sqrt{(\alpha_2 - d\theta_i)^2 - 4dg_i})/(2d),$$
$$\mu_-^{(i)}(d) = (\theta_i d - \alpha_2 - \sqrt{(\alpha_2 - d\theta_i)^2 - 4dg_i})/(2d).$$

Moreover, $H_i(d; \mu) < 0$ if and only if $\mu \in (\mu_-^{(i)}(d), \mu_+^{(i)}(d))$.

Theorem 4.2. *Assume that $\alpha_1 m_1 > \gamma_1$. Then the unique positive constant solution $(\hat{u}_1, \hat{v}_1)$ is locally asymptotically stable for the system (3.1) and (3.2), which means that we cannot expect that non-constant steady states bifurcate from the neighbourhood of the constant steady state E_1^*.*

Proof. Set

$$L = \begin{pmatrix} \Delta + \theta_1 & -\delta_1 \\ \alpha_2^2/\gamma_2 & d\Delta - \alpha_2 \end{pmatrix}.$$

For each $j \geq 0$, $\mathbf{X}_j$ is invariant under the operator L. ξ is an eigenvalue of L in $\mathbf{X}_j$ if and only if ξ is an eigenvalue of the matrix

$$\begin{pmatrix} -\mu_j + \theta_1 & -\delta_1 \\ \alpha_2^2/\gamma_2 & -d\mu_j - \alpha_2 \end{pmatrix}. \tag{4.9}$$

The characteristic equation of (4.9) takes the form

$$\xi^2 + \xi(\mu_j + d\mu_j - \theta_1 + \alpha_2) + H_1(d; \mu_j) = 0. \tag{4.10}$$

Since $\alpha_1 m_1 > \gamma_1$, then $\theta_1 < 0$ (see Appendix C). We further have $H_1(d; \mu_j) > 0$. It follows from the Routh–Hurwitz criterion that for each $j \geq 0$, the two eigenvalues ξ_{j1}, ξ_{j2} of (4.10) have negative real parts. By simple computation, there exists a positive constant δ such that $\mathrm{Re}\xi_{j1}, \mathrm{Re}\xi_{j2} < -\delta$. The assertion is obtained. □

Remark 4.1. The unique positive constant solution $(\hat{u}_1, \hat{v}_1)$ is globally asymptotically stable for the system (3.1) and (3.2) under the condition of $\alpha_1 m_1 > 2\gamma_1$ and $\gamma_2 > \alpha_2 m_1$. See Appendix D.

We now consider the case of two different constant steady states E_2^* and E_3^*, which are addressed in the following theorems.

Theorem 4.3. *Suppose the condition (4.4) and*

$$u^* > \hat{u}_3 \tag{4.11}$$

hold. If (4.8) is satisfied for some integers $0 \leq q < p$ and $m \geq 0$, then $\mu_-^{(3)}(d) \in (\mu_q, \mu_{q+1})$, $\mu_+^{(3)}(d) \in (\mu_p, \mu_{p+1})$ and $\mu_+^{(2)}(d) \in (\mu_m, \mu_{m+1})$. Denote $\sigma_p = \sum_{j=q+1}^{p} n(\mu_j)$, $\sigma_m = \sum_{j=0}^{m} n(\mu_j)$. Then the system (4.1) and (4.2) has at least one non-constant positive solution.

Proof. Since $u^* > \hat{u}_3$, we have $\theta_2 > \theta_3 > 0$. Moreover, since (4.8) holds and $g_3 > 0 > g_2$, we get

$$\mu_-^{(2)}(d) < 0, \quad \mu_-^{(3)}(d) > 0, \quad \mu_+^{(i)}(d) > 0, \quad i = 2, 3. \tag{4.12}$$

For some integers $0 \leq q < p$ and $m \geq 0$, by means of (4.12), we have

$$\mu_-^{(3)}(d) \in (\mu_q, \mu_{q+1}), \quad \mu_+^{(3)}(d) \in (\mu_p, \mu_{p+1}), \quad \mu_+^{(2)}(d) \in (\mu_m, \mu_{m+1}).$$

We shall show that the system (4.1) and (4.2) has at least one non-constant positive solution. On the contrary, suppose that this assertion is not true. In the following, we will derive a contradiction by using a homotopy argument.

For $t \in [0, 1]$, we define

$$G(\mathbf{w}; t) = \begin{pmatrix} u\left(\alpha_1 - \beta_1 u - \dfrac{t\gamma_1 v}{m_1 v + u}\right) \\ v\left(\alpha_2 - \dfrac{\gamma_2 v}{m_2 + u}\right) \end{pmatrix}$$

and consider the problem

$$-\Delta \mathbf{w} = D^{-1} G(\mathbf{w}; t). \tag{4.13}$$

Note that $\mathbf{w}$ is a non-constant positive solution of the model (4.1) and (4.2) if and only if it is a solution of the problem (4.13) for $t = 1$. On the other hand, for any $0 \leq t \leq 1$, $\mathbf{w}$ is a non-constant positive solution of the problem (4.13) if and only if it is a solution of the problem

$$h(\mathbf{w}; t) =: \mathbf{w} - (\mathbf{I} - \Delta)^{-1}\{D^{-1} G(\mathbf{w}; t) + \mathbf{w}\} \quad \text{on} \quad \mathbf{X}^+.$$

By Theorem 4.1, there exist positive constants $\underline{C}$ (Λ, Ω) and $\overline{C}(\Lambda, \Omega)$ such that for all $0 \leq t \leq 1$, the positive solutions of problem (4.13) satisfy $\underline{C} < u(x), v(x) < \overline{C}$ on $\bar{\Omega}$. Set

$$\sum = \{\mathbf{w} \in [C(\bar{\Omega})]^2 \mid \underline{C} < u(x), v(x) < \overline{C} \text{ on } \bar{\Omega}\}.$$

Then $h(\mathbf{w}; t) \neq 0$ for all $\mathbf{w} \in \partial\Sigma$ and $t \in [0, 1]$. By the homotopy invariance of the Leray–Schauder degree, it follows that

$$\deg\left(h(\cdot; 0), \sum, 0\right) = \deg\left(h(\cdot; 1), \sum, 0\right). \tag{4.14}$$

Since $h(\mathbf{w}; 1) = 0$ has only two positive solutions E_2^* and E_3^* in Σ, from Proposition 4.1, we have

$$\deg\left(h(\cdot; 1), \sum, 0\right) = \mathrm{index}(h(\cdot; 1), E_2^*) + \mathrm{index}(h(\cdot; 1), E_3^*) = (-1)^{\sigma_m} + (-1)^{\sigma_p}.$$

On the other hand, if $t = 0$, $h(\mathbf{w}; 0) = 0$ has only one positive solution $\mathbf{w}^*$ in Σ, similar to the front argument and making use of Proposition 4.1 again, we obtain

$$\deg\left(h(\cdot;0), \sum, 0\right) = \text{index}(h(\cdot;0), \mathbf{w}^*) = (-1)^0 = 1.$$

This is a contradiction to (4.14). The proof is completed. □

Corollary 4.1. *Suppose that (4.11) holds. If $\theta_3 \in (\mu_q, \mu_{q+1})$, $\theta_2 \in (\mu_p, \mu_{p+1})$ for some integer $0 \le q < p$. Denote $\sigma_p = \sum_{j=0}^{p} n(\mu_j)$, $\sigma_q = \sum_{j=1}^{q} n(\mu_j)$. Then there exists a positive constant d^* such that the system (4.1) and (4.2) has at least one non-constant positive solution for $d > d^*$.*

Theorem 4.4. *Suppose the condition (4.4) and*

$$\hat{u}_2 < u^* < \hat{u}_3 \tag{4.15}$$

hold. If (4.8) holds for some integer $m \ge 0$, $\mu_+^{(2)}(d) \in (\mu_m, \mu_{m+1})$. Denote $\sigma_m = \sum_{j=0}^{m} n(\mu_j)$. Then the system (4.1) and (4.2) has at least one non-constant positive solution.

Proof. Since $\hat{u}_2 < u^* < \hat{u}_3$, we have $\theta_3 < 0 < \theta_2$ (see Appendix C). Moreover, $g_3 > 0 > g_2$. Therefore, we obtain

$$\mu_-^{(2)}(d) < 0, \ \ \mu_+^{(2)}(d) \in (\mu_m, \mu_{m+1}).$$

Similar to the proof of Theorem 4.3, we have

$$\text{index}(h(\cdot;1), E_2^*) = \text{index}(f(d;\cdot), E_2^*) = (-1)^{\sigma_m}.$$

Since $\theta_3 < 0$ and $g_3 > 0$, we have $H_3(\,\cdot\,;\mu) > 0$ for all $\mu \ge 0$. It follows from Proposition 4.1 that

$$\text{index}(h(\cdot;1), E_3^*) = \text{index}(f(d;\cdot), E_3^*) = (-1)^0 = 1.$$

Thus,

$$\deg\left(h(\cdot;1), \sum, 0\right) = \text{index}(h(\cdot;1), E_2^*) + \text{index}(h(\cdot;1), E_3^*) = (-1)^{\sigma_m} + 1.$$

On the other hand, if $t = 0$, $h(\mathbf{w}; 0) = 0$ has only one positive solution $\mathbf{w}^*$ in Σ, making use of Proposition 4.1 again, we obtain

$$\deg\left(h(\cdot;0), \sum, 0\right) = \text{index}(h(\cdot;0), \mathbf{w}^*) = (-1)^0 = 1.$$

Therefore,

$$\deg\left(h(\cdot;0), \sum, 0\right) \ne \deg\left(h(\cdot;1), \sum, 0\right).$$

This proves our assertion. □

Corollary 4.2. *Suppose that (4.15) holds. If $\theta_2 \in (\mu_m, \mu_{m+1})$ for some integer $m \ge 0$. Denote $\sigma_m = \sum_{j=0}^{m} n(\mu_j)$. Then there exists a positive constant d^* such that the system (4.1) and (4.2) has at least one non-constant positive solution for $d > d^*$.*

Corollary 4.3. *Suppose that (4.11) or (4.15) holds. If $-g_2/\alpha_2 \in (\mu_m, \mu_{m+1})$ for some integer $m \ge 0$. Denote $\sigma_m = \sum_{j=0}^{m} n(\mu_j)$. Then there exists a positive constant d_* such that the system (4.1) and (4.2) has at least one non-constant positive solution for $0 < d < d_*$.*

Theorem 4.5. *Suppose the condition (4.4) and*

$$u^* < \hat{u}_2$$

hold. Then the two positive constant solutions $(\hat{u}_2, \hat{v}_2)$ and $(\hat{u}_3, \hat{v}_3)$ of the system (4.1) and (4.2) are locally asymptotically stable.

Proof. Since $u^* < \hat{u}_2$, we have $\theta_i < 0$ (see Appendix C), and we further have $g_i > 0$ $(i = 2, 3)$. Thus, we obtain $H_i(\cdot;\mu) > 0$ $(i = 2, 3)$ for all $\mu \ge 0$. Similar to the proof of Theorem 4.2, we can get the conclusion. □

5. Spatiotemporal bifurcations ($\Omega \subset R$)

In this section, we derive more precise conditions for the existence of non-constant steady state to the spatiotemporal system (3.1) and (3.2) with one dimension spatial domain in order to facilitate our numerical analysis in Section 6. We consider two cases: $\alpha_1 m_1 > \gamma_1$ and $\alpha_1 m_1 < \gamma_1$. In the former case, we show in Section 2 that the spatiotemporal model (3.1) and (3.2) has a unique constant steady state $E_1^* = (\hat{u}_1, \hat{v}_1)$ (see Eq. (2.3)) and in Section 4 that this constant steady state is locally asymptotically stable, which means that we cannot expect non-constant steady states (Theorem 4.2) around the neighbourhood of E_1^*. In the latter case, we further assume condition (2.4) holds to ensure the existence of the two different constant steady states $E_2^* = (\hat{u}_2, \hat{v}_2)$ and $E_3^* = (\hat{u}_3, \hat{v}_3)$ (see equations in (2.5)). There are three situations needed to

be considered: (1) $u^* < \hat{u}_2$, (2) $\hat{u}_2 < u^* < \hat{u}_3$, (3) $u^* > \hat{u}_3$, where u^* is given in (4.5). In fact, Theorem 4.5 shows that for the first situation both E_2^* and E_3^* are locally asymptotically stable, implying that non-constant steady state does not exist, leaving us with the other two situations, which will be addressed sequentially in the rest of this section (i.e., Theorems 5.1 and 5.2).

Without loss of generality, we take the space domain $\Omega = (0, l)$, $l > 0$. Thus, the system (3.1) and (3.2) and system (4.1) and (4.2) can be rewritten as

$$u_t = u\left(\alpha_1 - \beta_1 u - \frac{\gamma_1 v}{m_1 v + u}\right) + u_{xx}, \tag{5.1}$$

$$v_t = v\left(\alpha_2 - \frac{\gamma_2 v}{m_2 + u}\right) + d v_{xx}, \tag{5.2}$$

and

$$-u_{xx} = u\left(\alpha_1 - \beta_1 u - \frac{\gamma_1 v}{m_1 v + u}\right), \tag{5.3}$$

$$-d v_{xx} = v\left(\alpha_2 - \frac{\gamma_2 v}{m_2 + u}\right). \tag{5.4}$$

It is well known that the eigenvalues of the operator $-\partial/\partial x^2$ on $\Omega = (0, l)$ under the Neumann boundary condition are

$$\mu_j = \left(\frac{\pi j}{l}\right)^2, \quad j = 0, 1, 2, \cdots,$$

all of which are algebraically simple, and the corresponding eigenfunctions are given by

$$\phi_j(x) = \begin{cases} \dfrac{1}{\sqrt{l}}, & j = 0, \\ \sqrt{\dfrac{2}{l}} \cos\left(\dfrac{\pi j x}{l}\right), & j > 0. \end{cases}$$

Choosing d as the bifurcation parameter, we have the following linearized operator associated with the system (5.3) and (5.4) evaluated at $E_i^*(i = 1, 2, 3)$:

$$L(d) = \begin{pmatrix} \dfrac{\partial^2}{\partial x^2} + \theta_i & -\delta_i \\ \alpha_2^2/\gamma_2 & -d\dfrac{\partial^2}{\partial x^2} - \alpha_2 \end{pmatrix}.$$

It is easy to see that the eigenvalues of $L(d)$ are given by those of the following operator $L_j(d)$,

$$L_j(d) = \begin{pmatrix} -\mu_j + \theta_i & -\delta_i \\ \alpha_2^2/\gamma_2 & -d\mu_j - \alpha_2 \end{pmatrix},$$

whose characteristic equation is

$$\mu^2 - \mu T_{ij}(d) + D_{ij}(d) = 0, \tag{5.5}$$

where

$$T_{ij} = -(1 + d)\mu_j + \theta_i - \alpha_2, \quad D_{ij} = d\mu_j^2 + (\alpha_2 - d\theta_i)\mu_j + g_i, \tag{5.6}$$

where θ_i, δ_i and g_i can be found in (4.3).

According to [51], if there exist an integer $j_0 \geq 0$ and $d^H > 0$ such that

$$T_{ij_0}(d^H) = 0, \ D_{ij_0}(d^H) > 0, \ T_{ij}(d^H) \neq 0, \ D_{ij}(d^H) \neq 0, \ \text{for all } j \neq j_0 \tag{5.7}$$

and for the unique pair of complex eigenvalues $\alpha(d) \pm iw(d)$ of (5.5) near the imaginary axis, the derivative $\alpha'(d^H) \neq 0$. Then a Hopf bifurcation occurs at (d^H, E_i^*). This implies that close to the critical magnitude d^H, a family of spatially homogeneous or inhomogeneous periodic solutions of the system (5.1) and (5.2) emanates from the constant steady state E_i^*.

Also from [51], if there exist an integer $j_0 \geq 0$ and $d^S > 0$ such that

$$D_{ij_0}(d^S) = 0, \ T_{ij_0}(d^S) \neq 0, \ T_{ij}(d^S) \neq 0, \ D_{ij}(d^S) \neq 0, \ \text{for all } j \neq j_0, \tag{5.8}$$

and the derivative $D'_{ij_0}(d^S) \neq 0$, then a steady state bifurcation occurs at (d^S, E_i^*). This implies that close to the critical point d^S, a family of positive non-constant solutions of the model (5.3) and (5.4) emanates from the constant steady state E_i^*.

We have the following results regarding the stability of E_2^* and E_3^* as well as the existence of Hopf and steady state bifurcation, which are summarised in Theorems 5.1 and 5.2.

Theorem 5.1. *Assume condition (2.4) (i.e., Case C) and $u^* > \hat{u}_3$ hold. The following statements hold true*

(1) *Assume that* $\min\{\alpha_2, \mu_1\} < \theta_3 < \max\{\alpha_2, \mu_1\}$.

(a) *If additionally* $\alpha_2 < \mu_1$, *then* E_3^* *is unstable for any* $d > 0$.

(b) *If additionally* $\alpha_2 > \mu_1$, *let* J_0 *be the largest positive integer such that* $\theta_3 - \mu_j > 0$ *for any* $1 \le j \le J_0$. *Suppose that* $d_j \ne d_k$ *whenever* $j \ne k$, $1 \le j, k \le J_0$, *then for* $1 \le j \le J_0$ *the system (5.3) and (5.4) undergoes steady state bifurcation at* (d_j, E_3^*).

(2) *Assume that* $\max\{\alpha_2, \mu_1\} < \theta_3 < \alpha_2 + \mu_1$, *let* J_0 *be defined similarly as in* (1(b)), $\tilde{d} := \min_{1\le j\le J_0} d_j$ *and* $d_j \ne d_k$ *whenever* $j \ne k$, $1 \le j, k \le J_0$. *Then for* $1 \le j \le J_0$ *the system (5.3) and (5.4) undergoes steady state bifurcation at* (d_j, E_3^*). *However, for all* $0 < d < \tilde{d}$, E_3^* *is unstable.*

(3) *Assume that* $\alpha_2 + \mu_1 < \theta_3$.

(a) *Let* J_0 *be defined similarly as in* (1(b)) *and* $d_j \ne d_k$ *whenever* $j \ne k$, $1 \le j, k \le J_0$. *Then for* $1 \le j \le J_0$ *the system (5.3) and (5.4) undergoes steady state bifurcation at* (d_j, E_3^*).

(b) *Suppose that either*

$$\mu_1 > \max\left\{\theta_3 - \sqrt{\alpha_2\theta_3 + g_3}, \frac{\theta_3 - \alpha_2}{2}\right\}, \tag{5.9}$$

or

$$\mu_1 > \max\left\{\theta_3 - \sqrt{\alpha_2\theta_3 + g_3}, \frac{(\theta_3 - \alpha_2)\theta_3}{\alpha_2 + \theta_3}\right\}. \tag{5.10}$$

Then, the Hopf bifurcation occurs at (d_1^H, E_3^*) *if (5.9) holds or the Hopf bifurcation occurs at* (d_j^H, E_3^*) *for* $1 \le j \le J_0$ *if (5.10) holds, where*

$$d_j^H = \frac{\theta_3 - \alpha_2 - \mu_j}{\mu_j},$$

and J_0 *is the largest positive integer such that* $\theta_3 - \alpha_2 - \mu_j > 0$ *for any* $1 \le j \le J_0$. *Moreover, in either case, close to the critical point* d_j^H, *the system (5.1) and (5.2) has a family of inhomogeneous periodic solutions near* E_3^*.

Proof. We below prove the five statements in Theorem 5.1 sequentially.

Proof of statement 1a: Since $u^* > \hat{u}_3$, we have $\theta_3 > 0$. If $\alpha_2 < \mu_1$, the assumption $\min\{\alpha_2, \mu_1\} < \theta_3 < \max\{\alpha_2, \mu_1\}$ reads as $\alpha_2 < \theta_3 < \mu_1$. Then for all $d > 0$ and $j \ge 1$, by (5.6) we have

$$T_{3j}(d) = -(d\mu_j + \alpha_2) + \theta_3 - \mu_j < 0.$$

However, $T_{30}(d) = \theta_3 - \alpha_2 > 0$. On the other hand,

$$D_{3j}(d) = d\mu_j(\mu_j - \theta_3) + \alpha_2\mu_j + g_3 > 0$$

for all $j \ge 1$ and $d > 0$ since $g_3 > 0$ and $\theta_3 < \mu_1$ when case C holds. Moreover, $D_{30}(d) = g_3 > 0$ and $T_{30}(d) > 0$. Thus, there exists a pair of eigenvalues having positive real parts, and all the other eigenvalues have negative real parts. This shows that E_3^* is linearly unstable for the system (5.1) and (5.2) for any given $d > 0$.

Proof of statement 1b: Again, we have $\theta_3 > 0$. If $\alpha_2 > \mu_1$, the assumption $\min\{\alpha_2, \mu_1\} < \theta_3 < \max\{\alpha_2, \mu_1\}$ reads as $\mu_1 < \theta_3 < \alpha_2$. We have

$$T_{3j}(d) = -\mu_j(1 + d) + \theta_3 - \alpha_2 < 0$$

for all $j \ge 0$ and $d > 0$. Furthermore, by the definition of J_0, we have $\theta_3 - \mu_j > 0$ if $1 \le j \le J_0$. Hence, for any $1 \le j \le J_0$, d_j is well defined. We additionally have $d_j > 0$ and $D_{3j}(d_j) = 0$. By the assumption $d_j \ne d_k$ whenever $j \ne k$, $1 \le j, k \le J_0$, it is easy to see that $D_{3k}(d_j) \ne 0$ for $j, k \ge 1$, $j \ne k$. Finally, when $1 \le j \le J_0$, there holds

$$D'_{3j}(d_j) = \mu_j(\mu_j - \theta_3) \ne 0.$$

Therefore, for fixed $1 \le j \le J_0$ the system (5.3) and (5.4) undergoes steady state bifurcation at (d_j, E_3^*).

Proof of statement 2: The proof of the existence of steady state bifurcation is similar to that of 1(b) and we omit the details. Here we only verify the second part of statement (2). In fact, for all $d < \tilde{d}$, we have $D_{3j}(d) > 0$ and $T_{3j}(d) < 0$ for $j \ge 1$. Moreover, $D_{30}(d) > 0$ and $T_{30}(d) > 0$. This implies that there exists a pair of eigenvalues having positive real parts and all the others have negative real parts. Thus, for all $0 < d < \tilde{d}$, E_3^* is unstable.

Proof of statement 3a: The verification of steady state bifurcation is similar to that of statement (1(b)) and (2). We are going to prove the existence of Hopf bifurcation. We first assume that (5.9) holds. Clearly, $T_{31}(d_1^H) = 0$, $T_{3j}(d_1^H) \ne 0$ for $j \ge 2$ and $T_{30}(d) = \theta_3 - \alpha_2 > 0$. In addition, we note that $D_{30}(d) = g_3 \ne 0$ for any $d > 0$. Thus in (5.7) we need to check $D_{31}(d_1^H) > 0$ and $D_{3j}(d_1^H) \ne 0$ for all $j \ge 2$. In fact, in view of the expressions of d_1^H and $D_{31}(d_1^H)$, the former is equivalent to

$$\mu_1^2 - 2\mu_1\theta_3 - \alpha_2\theta_3 - g_3 + \theta_3^2 < 0,$$

which is fulfilled by the condition $\mu_1 > \theta_3 - \sqrt{\alpha_2\theta_3 + g_3}$. On the other hand, by elementary calculation, one can easily see that the condition $\mu_1 > (\theta_3 - \alpha_2)/2$ guarantees $2\mu_1^2 - \mu_1(3\theta_3 - \alpha_2) + \theta_3^2 - \alpha_2\theta_3 < 0$ for $\mu > \mu_1$, which therefore

shows $D_{3j}(d_1^H)$ is nondecreasing with respect to $j \geq 1$. Hence, when $j \geq 2$, $D_{3j}(d_1^H) \geq D_{31}(d_1^H) > 0$. Furthermore, by solving (5.5) for $j = 1$ near $d = d_1^H$, we get conjugate complex eigenvalue

$$\mu = \frac{1}{2}\left\{T_{31}(d) \pm i\sqrt{4D_{31}(d) - T_{31}^2(d)}\right\}.$$

Then, the real part $\alpha(d) = T_{31}(d)/2$. Thus, the derivative

$$\alpha'(d_1^H) = \frac{1}{2}T'_{31}(d_1^H) = -\frac{1}{2}\mu_1 \neq 0.$$

As a consequence, Hopf bifurcation occurs at (d_1^H, E_3^*), which also implies that the system (5.1) and (5.2) has a family of inhomogeneous periodic solutions near E_3^*.

Proof of statement 3b: Similar to the proof of statement (3a), we only prove the existence of Hopf bifurcation. We assume that (5.10) holds. By the definition of d_j^H, we have $T_{3j}(d_j^H) = 0$ and $T_{3k}(d_j^H) \neq 0$ whenever $j \neq k$ and $1 \leq j, k \leq J_0$. Moreover, for any $d > 0$, $T_{30}(d) > 0$ and $D_{30}(d) \neq 0$. We next show that for fixed k with $1 \leq j \leq J_0$, $D_{3k}(d_j^H) > 0$ if $k \geq 1$. Indeed, from (5.10) we have $d_j^H\theta_3 < \alpha_2$ and $D_{31}(d_1^H) > 0$, which then implies that for $1 \leq j \leq J_0$ and $k \geq 1$, we have

$$D_{3k}(d_j^H) = d_j^H\mu_k^2 + \mu_k(\alpha_2 - d_j^H\theta_3) + g_3 > 0.$$

On the other hand, as above, when $1 \leq j \leq J_0$, we get $\alpha'(d_j^H) = -\frac{1}{2}\mu_j \neq 0$ and so the transversality condition holds. Consequently, we can conclude that under (5.10), Hopf bifurcation occurs at (d_j^H, E_3^*) for any fixed $1 \leq j \leq J_0$. □

Theorem 5.2. *Assume condition (2.4) (i.e., Case C) holds, and additionally suppose that*

$$\hat{u}_2 < u^* < \hat{u}_3, \ g_2 > -\alpha_2\mu_1.$$

The following statements hold true:

(1) *E_3^* is locally asymptotically stable for any $d > 0$.*

(2) *Assume that $\min\{\alpha_2, \mu_1\} < \theta_2 < \max\{\alpha_2, \mu_1\}$.*

(a) *If additionally $\alpha_2 < \mu_1$, then E_2^* is unstable for any $d > 0$.*

(b) *If additionally $\alpha_2 > \mu_1$, let J_0 be the largest positive integer such that $\theta_2 - \mu_j > 0$ for any $1 \leq j \leq J_0$. Suppose that $d_j \neq d_k$ whenever $j \neq k$, $1 \leq j, k \leq J_0$, then for $1 \leq j \leq J_0$ the system (5.3) and (5.4) undergoes steady state bifurcation at (d_j, E_2^*).*

(3) *Assume that $\max\{\alpha_2, \mu_1\} < \theta_2 < \alpha_2 + \mu_1$. J_0 is defined in the way as in (2(b)). Let $\tilde{d} := \min_{1\leq j\leq J_0} d_j$ and $d_j \neq d_k$ whenever $j \neq k$, $1 \leq j, k \leq J_0$. Then for $1 \leq j \leq J_0$ the system (5.3) and (5.4) undergoes steady state bifurcation at (d_j, E_2^*). However, for all $0 < d < \tilde{d}$, E_2^* is unstable.*

(4) *Assume that $\alpha_2 + \mu_1 < \theta_2$.*

(a) *Let J_0 be defined similarly as in (2) and $d_j \neq d_k$ whenever $j \neq k$, $1 \leq j, k \leq J_0$. Then for $1 \leq j \leq J_0$ the system (5.3) and (5.4) undergoes steady state bifurcation at (d_j, E_2^*).*

(b) *Suppose that either*

$$\mu_1 > \max\left\{\theta_2 - \sqrt{\alpha_2\theta_2 + g_2}, \frac{\theta_2 - \alpha_2}{2}\right\} \tag{5.11}$$

or

$$\mu_1 > \max\left\{\theta_2 - \sqrt{\alpha_2\theta_2 + g_2}, \frac{(\theta_2 - \alpha_2)\theta_2}{\alpha_2 + \theta_2}\right\} \tag{5.12}$$

holds. Then Hopf bifurcation occurs at (d_1^H, E_2^*) under condition (5.11) or Hopf bifurcation occurs at (d_j^H, E_2^*) for $1 \leq j \leq J_0$ under condition (5.12), where

$$d_j^H = \frac{\theta_2 - \alpha_2 - \mu_j}{\mu_j}, \tag{5.13}$$

and J_0 is the largest positive integer such that $\theta_2 - \alpha_2 - \mu_j > 0$ for any $1 \leq j \leq J_0$. Moreover, in either case, close to the critical point d_j^H, the system (5.1) and (5.2) has a family of inhomogeneous periodic solutions near E_2^*.

The proof of Theorem 5.2 is similar to the argument of Theorem 5.1 and hence omitted.

6. Numerical results

This section is devoted to numerically verifying the conditions ensuring the existence of non-constant steady states presented in Theorem 5.1 and the comparison of these conditions to those guaranteeing the existence of Turing patterns. We are interested in this theorem because Turing instability occurs only around the constant steady state E_3^* (Section 2). To this aim, we consider one dimensional spatial domain $\Omega \equiv (0, l)$ with l being given later to meet the requirements on the

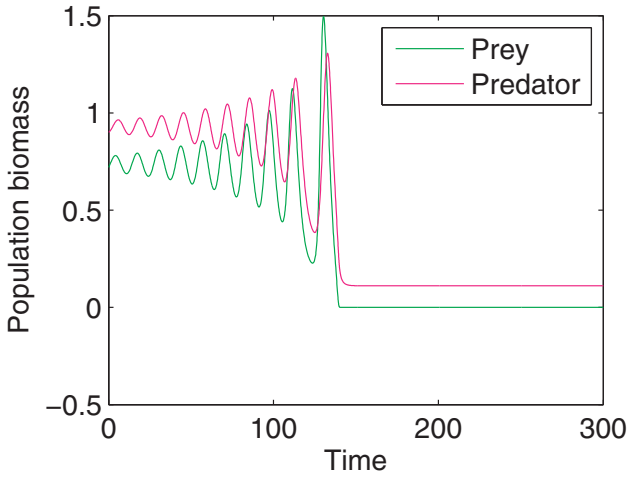

Fig. 4. Spatiotemporal dynamics unfold spirally until the extinction of the prey. Parameter values are $\alpha_2 = 0.5,\ \gamma_1 = 1.4,\ l = 2$ and $d = 1$.

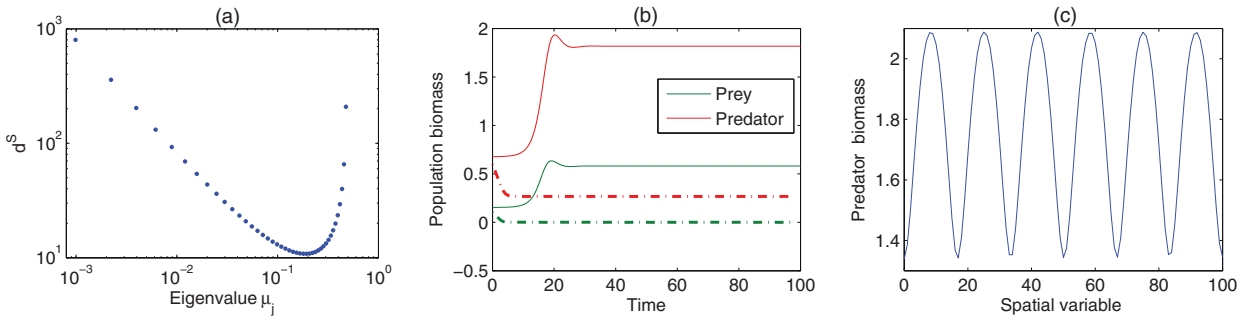

Fig. 5. Critical diffusion rates for the steady state bifurcation over varied eigenvalues (a), population dynamics with (solid) and without (dashed) diffusion (b), and emergent stationary spatial pattern (c). Parameter values are $\alpha_2 = 1.2,\ \gamma_1 = 0.8,\ d = 15$ and $l = 100$.

eigenvalue $\mu_1 = (\pi/l)^2$. There are five statements in Theorem 5.1, and we below verify them sequentially. To begin with, we fix the parameters $\alpha_1 = 2,\ \beta_1 = 0.8,\ \gamma_2 = 0.45,\ m_1 = 0.2,\ m_2 = 0.1$, and vary α_2, γ_1, l and d.

For the statement (1a) in Theorem 5.1, we choose $\alpha_2 = 0.5,\ \gamma_1 = 1.4$ and $l = 2$. Direct calculation shows that $\theta_3 = 0.5371$ and $\mu_1 = 2.4674$, which implies $\alpha_2 < \theta_3 < \mu_1$. Thus, $\hat{\mathbf{u}}_3 = (0.7366, 0.9296)$ is unstable for any $d > 0$. Numerical simulation shows that small random perturbations around the equilibrium solution lead to extinction of prey in the spatiotemporal model (5.1) and (5.2) (Fig. 4).

For the statement (1b) in Theorem 5.1, we choose $\alpha_2 = 1.2,\ \gamma_1 = 0.8$ and $l = 100$. Direct calculation shows that $\theta_3 = 0.4873,\ \mu_1 = 0.0009869$, and $\hat{\mathbf{u}}_3 = (0.5748, 1.7995)$. It is easy to see that $\mu_1 < \theta_3 < \alpha_2$. From equations (5.6) and (5.7) we find a set of steady state bifurcation points (Fig. 5a). The minimum diffusion rate required for steady state bifurcation to occur is $d^S = 10.8285$. Interestingly, diffusion facilitates the coexistence of prey and predator, which is however impossible in the absence of diffusion (Fig. 5b). The emergent spatial pattern with $d = 15$ is stationary (Fig. 5c). In addition, we do not find any Hopf bifurcation according to the condition (5.7).

For the statement (2) in Theorem 5.1, we choose $\alpha_2 = 0.6,\ \gamma_1 = 1.3$ and $l = 4$, which yield that $\theta_3 = 0.7394,\ \mu_1 = 0.6169$ and $\hat{\mathbf{u}}_3 = (0.5551, 0.8734)$. It is easy to see that $\max\{\alpha_2, \mu_1\} < \theta_3 < \theta_2 < \alpha_2 + \mu_1$. We additionally find that $J_0 = 1$ and $d_1^S = 6.9855$. Thus according to this theorem, the system (5.3) and (5.4) undergoes steady state bifurcation at (d_1^S, E_3^*) and E_3^* is unstable for any $0 < d < d_1^S$. We perform extensive numerical simulation but do not observe any stationary or non-stationary spatial patterns. In all performed simulations, prey species always goes to extinction. One reason might be that the non-constant steady state bifurcating from E_3^* is unstable and cannot be captured numerically. Finally direct computation shows that there is no any Hopf bifurcation.

For the statement (3) in Theorem 5.2, we choose $\alpha_2 = 0.12,\ \gamma_1 = 5$ and $l = 100$, which give rise to $\theta_3 = 0.7870$, and $\mu_1 = 0.0009869$ and $\hat{\mathbf{u}}_3 = (0.7067, 0.2151)$. It is easy to see that $\alpha_2 + \mu_1 < \theta_3$. We find that $J_0^S = 28$ and the critical diffusion rates d_j^S $(j = 1, \cdots, J_0^S)$ from condition (5.8) (Fig. 6a). According to the predictions by Theorem 5.2, the system (5.3) and (5.4) undergoes steady state bifurcation at (d_j^S, E_3^*), with the minimum critical diffusion rate $d_{17}^S = 0.5726$ and $\mu_{17} = 0.2852$. Furthermore, we calculate the critical diffusion rate d^H for Hopf bifurcation from condition (5.7) under the same set of parameter values. There are in total 25 critical diffusion rates meeting condition $T_{3j}(d_j^H) = 0$, and among them only 5 critical

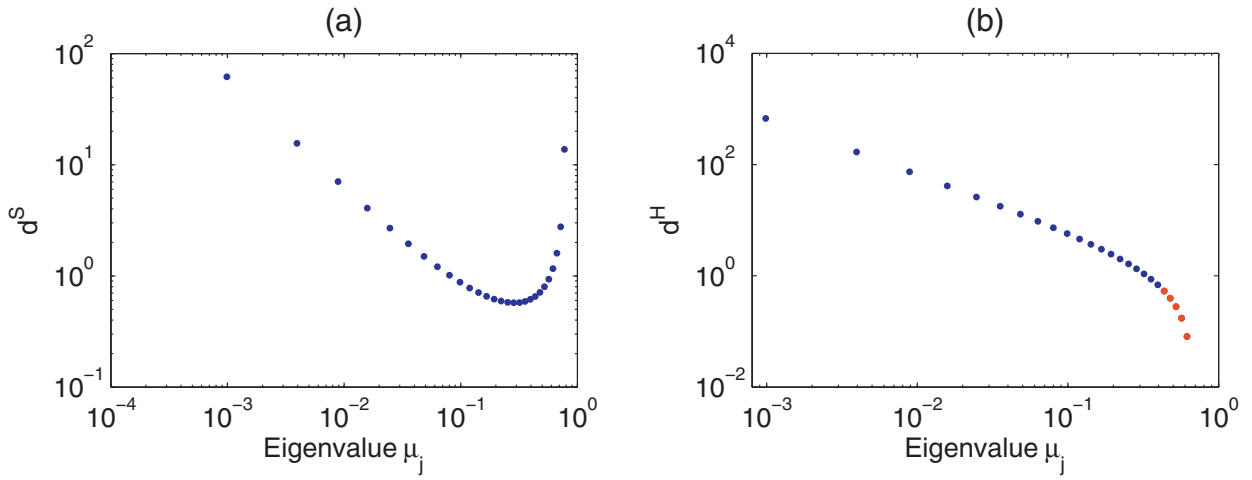

Fig. 6. Critical diffusion rates for the steady state bifurcation (a) and Hopf bifurcation (b) as a function of the eigenvalue $\mu_j = (j\pi/l)$, which are, respectively, calculated from conditions (5.8) and (5.7). In the right panel, red dots are Hopf bifurcation points. The blue dots are not Hopf bifurcation points, but they satisfy equation $T_j(d_j^H) = 0$ in (5.7). Parameter values are $\alpha_2 = 0.12$, $\gamma_1 = 5$ and $l = 100$.(For interpretation of the references to colour in this figure legend, the reader is referred to the web version of this article.)

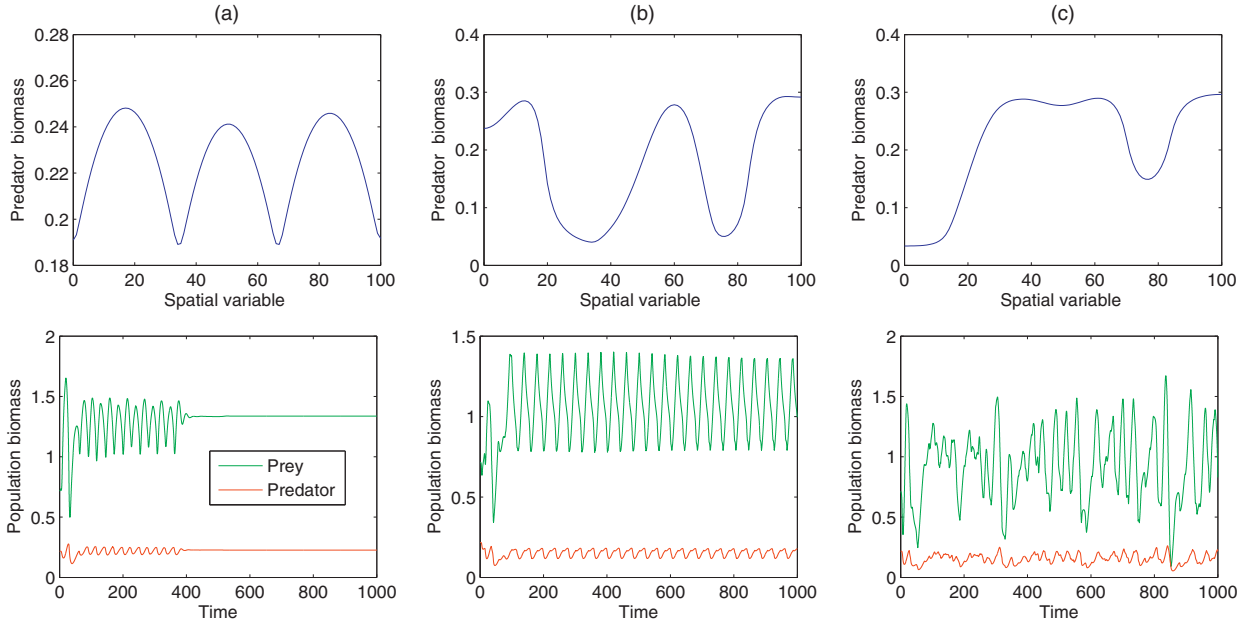

Fig. 7. Examples of spatial patterns (snapshots at the exhibited final time) and spatially averaged population dynamics for $d = 30$ (left), $d = 2$ (middle), $d = 4$ (right). $\alpha_2 = 0.12$, $\gamma_1 = 5$ and $l = 100$.

diffusion rates are Hopf bifurcation points (Fig. 6b), which are $d_j^H = (0.5325, 0.3963, 0.2775, 0.1733, 0.0813)$ and their associated eigenvalues are $\mu_j = (0.4352, 0.4777, 0.5221, 0.5685, 0.6169)$ for $j = 21, 22, 23, 24, 25$. Here we do not follow the statement (3b) in Theorem 5.1 because the condition is too strong. In fact, the conditions in (5.9) and/or (5.10) guarantee that the first positive eigenvalue is a bifurcation point, which is however not necessary (see from Fig. 6b).

We perform detailed numerical simulations with respect to the system (5.1) and (5.2) by disturbing the system initially settling at its steady state E_3^* with a small random noise for different values of diffusion rate d. We find that non-stationary patterns arise for small diffusion rates while stationary patterns arise only when the diffusion rate is sufficiently large (Fig. 7). We further find that different initial conditions with the same diffusion rate $d = 30$ can lead to the emergence of different spatial patterns that can be stationary, periodic and chaotic (Fig. 8). This implies that there are alternative non-constant steady states, which can be stable or unstable. From Figs. 7a and 8a, we can see that there are at least two stationary non-constant steady states for the same set of parameter values.

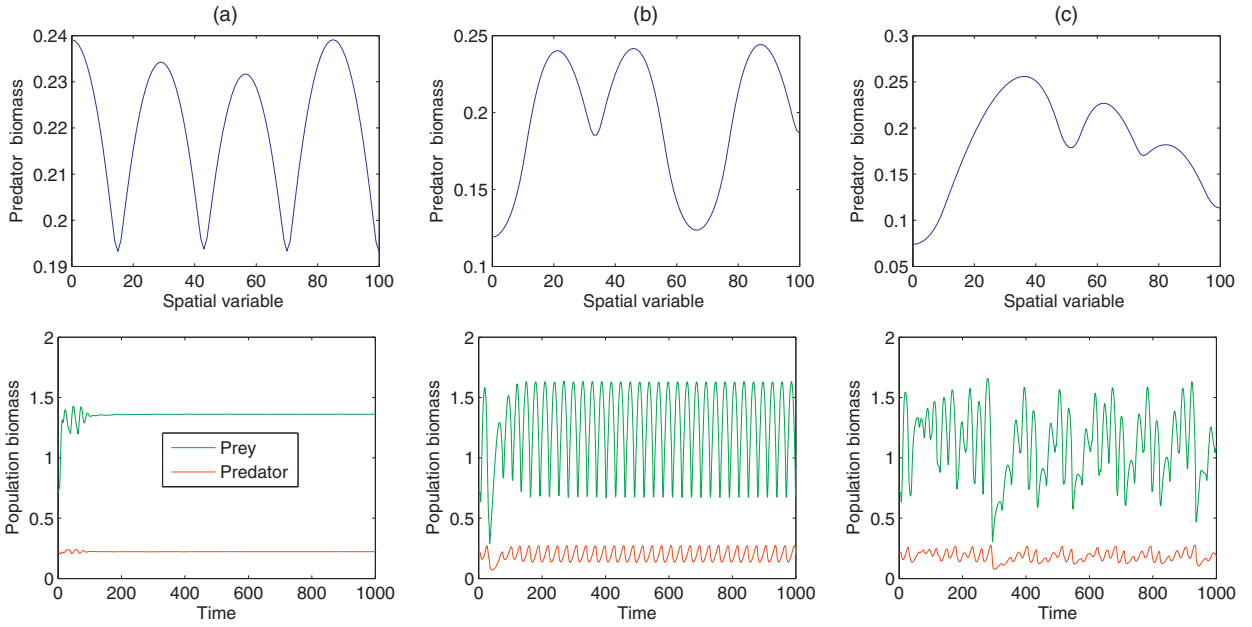

Fig. 8. Examples of spatial patterns (snapshots at the exhibited final time) and spatially averaged population dynamics for different random perturbed initial conditions with the same diffusion rate of $d = 30$. Parameter values are $\alpha_2 = 0.12$, $\gamma_1 = 5$ and $l = 100$.

As we see from Theorem 5.1, the parameters α_2 and θ_3 have a decisive role in determining the steady state bifurcation and Hopf bifurcation around the constant steady state E_3^*. We illustrate in Fig. 9 the regions where $\alpha_2 < \theta_3$ (denoted by T_1) and $\alpha_2 > \theta_3$ (part of this region is denoted by T_2). In the region T_1, Theorem 5.1 shows that both steady state bifurcation and Hopf bifurcation can occur. Interestingly, the region T_1 coincides with the region where E_3^* undergoes Hopf bifurcation in the temporal system (2.1) and (2.2) (see Fig. 1). In the region T_2, we only find steady state bifurcations around the constant steady state E_3^*. The orange square in Fig. 9 meets the statement (1b) of Theorem 5.1 and for the parameters associated with this orange square we only see stationary spatial patterns (e.g., Fig. 5c). However, we find that this region is identical to the region where Turing instability takes place (see Fig. 2).

7. Conclusions

There are four findings. First, we found that in the focal parameter space spanned by γ_1 and α_2, the region where Turing instability occurs (Fig. 2) is identical to the region where steady state bifurcation occurs only (i.e., T_2 in Fig. 9). This finding implies that Turing pattern is a stable non-constant steady state. However, a stable non-constant steady state might not be a Turing pattern since we observe both stable and unstable non-constant steady state in the region T_1 (see the purple square in Figs. 9 and 8). Recall that a necessary condition for Turing pattern is a stable local kinetic dynamics (i.e., stable equilibrium) and notice that a stable non-constant steady state can bifurcate from an unstable constant steady state. Thus, we conclude that Turing patterns are stable non-constant steady states bifurcating from stable constant steady state.

Second, in region T_2 (Fig. 9), we found both steady state bifurcation and Hopf bifurcation. The steady state bifurcation implies the existence of non-constant steady state to the system (5.1) and (5.2). The Hopf bifurcation implies that the non-constant steady state might be unstable. The net effect between the destabilising effects of Hopf bifurcation and the stabilising effects of diffusion determines the stability of the non-constant steady state. Generally, destabilising effect is dominant when diffusion rate is small while stabilising effect is dominant when diffusion rate is sufficiently large. This explains why we observed stationary spatial patterns only with large diffusion rate and non-stationary spatial patterns with small diffusion rate in Fig. 7.

Third, there exist alternative non-constant steady states under the same parameter set. Our numerical simulations show that there are two different stationary spatial patterns (Figs. 7a and 8a), one temporally oscillating spatial patterns (Fig. 8b) and one spatiotemporal chaos (Fig. 8c). Thus there are two stable non-constant steady states and two unstable non-constant steady states. Which spatial pattern emerges depends on which attracting basin of the four constant-steady states the initial condition will fall into. We conclude that coupling diffusion into a temporal model can enrich the population dynamics significantly, in particular when interacting with different kinds of bifurcations (e.g. Hopf bifurcation and Homoclinic bifurcation in Fig. 1).

Finally, we found that the mobility of individuals for both species within their habitat can promote the coexistence of prey and predator (see Fig. 5b).

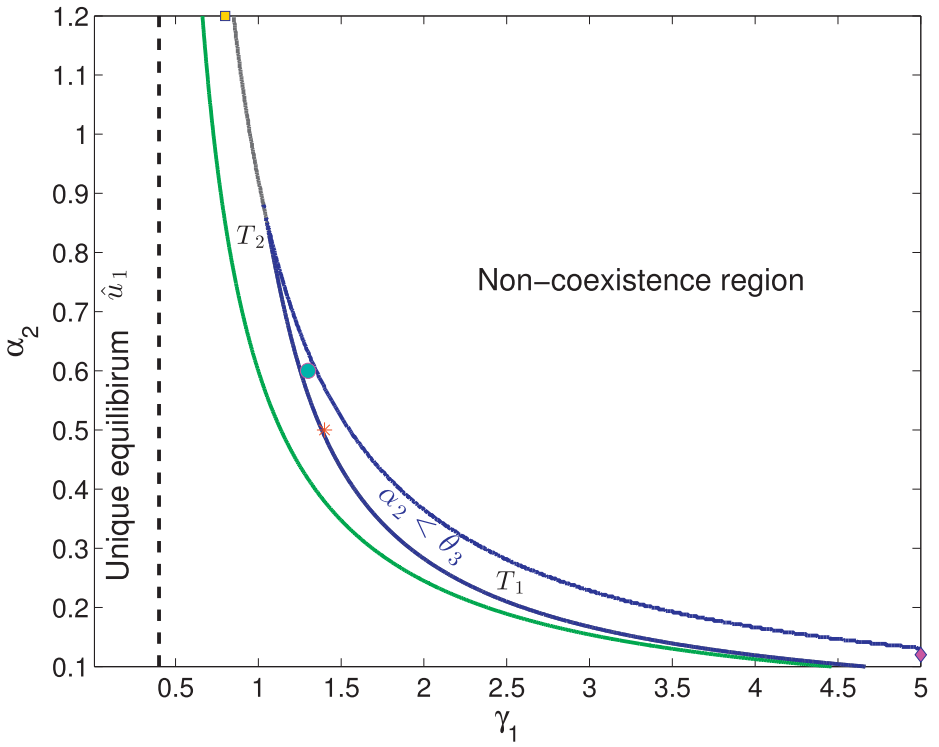

Fig. 9. Diagram of steady state and Hopf bifurcations in the spatiotemporal system (5.1) and (5.2). The region $\alpha_2 < \theta_3$ is surrounded by blue curves (i.e., the region T_1), while the region $\alpha_2 > \theta_3$ is a combination of the region T_2 and the region bounded from the right of the vertical dashed line and from the left of the green curve. The region T_1 is also the region where the equilibrium $\hat{\mathbf{u}}_3$ is locally unstable for the temporal system (2.1) and (2.2). The region given by T_2 is where $\hat{\mathbf{u}}_3$ is locally stable but Turing unstable. The black curve (partly covered by the blue curve) is the saddle node bifurcation curve, to the right of which there are no positive constant steady states. The green curve means $u^* = \hat{u}_3$, to the right of which $u^* > \hat{u}_3$ wherever $\hat{\mathbf{u}}_3$ is feasible. The symbols (orange square $(\gamma_1, \alpha_2) = (0.8, 1.2)$, light blue cycle $(\gamma_1, \alpha_2) = (0.6, 1.3)$, red star $(\gamma_1, \alpha_2) = (0.5, 1.4)$ and magenta diamond $(\gamma_1, \alpha_2) = (5, 0.12)$) are four examples, respectively meeting the four statements in Theorem 5.1. Parameter values are $\alpha_1 = 2$, $\beta_1 = 0.8$, $\gamma_1 = 1.4$, $\gamma_2 = 0.45$, $m_1 = 0.2$, $m_2 = 0.1$. (For interpretation of the references to colour in this figure legend, the reader is referred to the web version of this article.)

Acknowledgment

Lai Zhang gratefully acknowledges the financial support from the Swedish Strategic Research Programme eSSENCE, the Science and Technology Program of Nantong (BK2014063), and the PRC Grant NSFC 11571301.

Appendix A. Standard Turing analysis around E_1^*

In order to obtain the conditions for the Turing instability to occur in the system (3.1) and (3.2), one should check how a small heterogeneous perturbation from the homogeneous steady state develops in the large-time limit. For this purpose, we consider the following perturbation

$$u(x, y, t) = \hat{u}_i + \epsilon \exp[(\kappa_x x + \kappa_y y) j + \mu_\kappa t], \tag{A.1}$$

$$v(x, y, t) = \hat{v}_i + \delta \exp[(\kappa_x x + \kappa_y y) j + \mu_\kappa t], \tag{A.2}$$

where ϵ and δ are chosen to be small and $\kappa = (\kappa_x, \kappa_y)$ is the wave number. Substituting (A.1) and (A.2) into (3.1) and (3.2), linearizing the system around the interior equilibrium $(\hat{u}_i, \hat{v}_i)(i = 1, 2, 3)$ and considering the conditions when at least one of the eigenvalues of the linearized system crosses the imaginary axis, we obtain the following instability condition

$$h(\kappa^2) = d(\kappa^2)^2 + \kappa^2(\alpha_2 - d\theta_i) + g_i < 0,$$

where

$$\theta_i = \frac{\gamma_1 \hat{u}_i \hat{v}_i}{(m_1 \hat{v}_i + \hat{u}_i)^2} - \beta_1 \hat{u}_i, \quad \delta_i = \frac{\gamma_1 (\hat{u}_i)^2}{(m_1 \hat{v}_i + \hat{u}_i)^2}, \quad g_i = \delta_j \alpha_2^2 / \gamma_2 - \alpha_2 \theta_i.$$

Note that g_i is actually the determinant of the Jacobian matrix J_i for the system (2.1) and (2.2) that is evaluated at the constant steady state E_i^*, where

$$J_i = \begin{pmatrix} \theta_i & -\delta_i \\ \alpha_2^2/\gamma_2 & -\alpha_2 \end{pmatrix}.$$

Moreover, after simple algebraic calculation, we have that $g_1 > 0$ under Case B and $g_3 > 0$ ($g_2 < 0$) under Case C.

The minimum of $h(\kappa^2)$ occurs at $\kappa^2 = \kappa_{cr}^2$, where

$$\kappa_{cr}^2 = \frac{d\theta_i - \alpha_2}{2d} > 0. \tag{A.3}$$

Thus, a sufficient condition for instability is that $h(\kappa_{cr}^2) < 0$, that is,

$$h(\kappa_{cr}^2) = g_i - (\alpha_2 - d\theta_i)^2/(4d) < 0. \tag{A.4}$$

From (A.3) and (A.4), we obtain the following final criterion for diffusive instability

$$d\theta_i - \alpha_2 > 2\sqrt{g_i d} > 0. \tag{A.5}$$

Thus, the threshold condition for the occurrence of diffusive instability is

$$d\theta_i - \alpha_2 = 2\sqrt{g_i d}.$$

From the inequality (A.5) we see that θ_i ($i = 1, 2, 3$) must be positive in order to make this inequality valid due to the fact of $\alpha_2 > 0$. However we find that $\theta_1 < 0$ is automatically satisfied under Case B, and hence Turing instability does not happen around E_1^*.

Appendix B. Proof of Theorem 4.1

To prove Theorem 4.1 we need to give a priori estimates for the positive upper and lower bounds for positive solutions of the system (4.1) and (4.2). We first state the following two lemmas [17,19].

Lemma B.1 (Maximum principle). *Suppose that $g \in C(\bar{\Omega} \times \mathcal{R}^1)$,* (i) *Assume that $\omega(x) \in C^2(\Omega) \cap C^1(\bar{\Omega})$ and satisfies*

$$\Delta\omega(x) + g(x, \omega(x)) \geq 0, \quad x \in \Omega; \qquad \partial_\eta \omega \leq 0, \quad x \in \partial\Omega.$$

If $\omega(x_0) = \max_{\bar{\Omega}} \omega(x)$, then $g(x_0, \omega(x_0)) \geq 0$.

(ii) *Assume that $\omega(x) \in C^2(\Omega) \cap C^1(\bar{\Omega})$ and satisfies*

$$\Delta\omega(x) + g(x, \omega(x)) \leq 0, \quad x \in \Omega; \qquad \partial_\eta \omega \geq 0, \quad x \in \partial\Omega.$$

If $\omega(x_0) = \min_{\bar{\Omega}} \omega(x)$, then $g(x_0, \omega(x_0)) \leq 0$.

Lemma B.2 (Harnack inequality). *Assume that $c(x) \in C(\bar{\Omega})$ and let $\omega \in C^2(\Omega) \cap C^1(\bar{\Omega})$ be a positive solution of*

$$\Delta\omega(x) + c(x)\omega(x) = 0, \quad x \in \Omega; \qquad \partial_\eta \omega = 0, \quad x \in \partial\Omega.$$

Then there exists a positive constant $C_* = C_*(\| c(x) \|_\infty, \Omega)$ such that

$$\max_{\bar{\Omega}} \omega \leq C_* \min_{\bar{\Omega}} \omega.$$

Now we are in a position to prove the Theorem 4.1. The simple comparison argument and Lemma B.1 show that

$$u(x) < \alpha_1/\beta_1, \ \ v(x) < \alpha_2(\beta_1 m_2 + \alpha_1)/(\beta_1\gamma_2), \ \ v(x) > \alpha_2 m_2/\gamma_2. \tag{B.1}$$

Now, it suffices to verify the lower bound of u. We shall prove it by contradiction argument.

Suppose that the positive lower bound of u does not exist, then there exist a sequence $\{d_i\}_{i=1}^\infty$ and the positive non-constant solution (u_i, v_i) corresponding to $d = d_i$ such that

$$\min_{\bar{\Omega}} u_i(x) \to 0 \quad \text{as} \quad i \to \infty, \tag{B.2}$$

and (u_i, v_i) satisfies

$$\begin{cases} -\Delta u_i = u_i\left(\alpha_1 - \beta_1 u_i - \dfrac{\gamma_1 v_i}{m_1 v_i + u_i}\right), \\ -d_i \Delta v_i = v_i\left(\alpha_2 - \dfrac{\gamma_2 v_i}{m_2 + u_i}\right). \end{cases} \tag{B.3}$$

Furthermore, the following holds

$$\left\| \alpha_1 - \beta_1 u_i - \frac{\gamma_1 v_i}{m_1 v_i + u_i} \right\|_\infty \leq 2\alpha_1 + \frac{\gamma_1}{m_1}, \quad \forall i \geq 1. \tag{B.4}$$

Here and in what follows, $\|\cdot\|$ means the usual maximal norm over Ω.

On the other hand, from the first equation of (B.3), Lemma B.2, and the inequality (B.4), we can conclude that there is a positive constant $C = C(\Lambda, \Omega)$ such that

$$\max_{\bar{\Omega}} u_i(x) \le C \min_{\bar{\Omega}} u_i(x).$$

Combining with (B.2) gives

$$u_i(x) \to 0 \quad \text{uniformly} \quad \text{on} \quad \bar{\Omega}, \quad \text{as} \quad i \to \infty. \tag{B.5}$$

By integrating the first equation in problem (B.3), we get

$$\int_\Omega u_i\Big(\alpha_1 - \beta_1 u_i - \frac{\gamma_1 v_i}{m_1 v_i + u_i}\Big)\mathrm{d}x = 0.$$

Therefore, for each $i \ge 1$, there exists $x_i \in \bar{\Omega}$ such that

$$\alpha_1 - \beta_1 u_i(x_i) - \frac{\gamma_1 v_i(x_i)}{m_1 v_i(x_i) + u_i(x_i)} = 0. \tag{B.6}$$

The embedding theory and the standard regularity theory of elliptic equations guarantee the existence of a subsequence $\{(u_i, v_i)\}$, and two non-negative functions $u, v \in C^2(\bar{\Omega})$, such that $(u_i, v_i) \to (u, v)$ in $[C^2(\bar{\Omega})]^2$ as $i \to \infty$. Since (u_i, v_i) satisfies (B.6), so does (u, v). In virtue of (B.1) and (B.5), we obtain that $u = 0, v \ne 0$ uniformly on $\bar{\Omega}$. Let $i \to \infty$ in (B.6), and we obtain $\alpha_1 m_1 = \gamma_1$, which is a contradiction with our assumption. This completes the proof.

Appendix C. Relationship between θ_1, θ_2, and θ_3

The relationship can be formulated as follows:

(i) If $\alpha_1 m_1 > \gamma_1$, then $\theta_1 < 0$.

(ii) If $\alpha_1 m_1 < \gamma_1$ and (2.4) hold, then

(1) $\theta_3 < \theta_2 < 0$ when $u^* < \hat{u}_2$; (2) $\theta_3 < 0 < \theta_2$ when $\hat{u}_2 < u^* < \hat{u}_3$; (3) $\theta_2 > \theta_3 > 0$ when $u^* > \hat{u}_3$,

where $u^* = \frac{\alpha_1 m_1 - \gamma_1 + \sqrt{\gamma_1(\gamma_1 - \alpha_1 m_1)}}{m_1 \beta_1}$.

We now prove the first statement. Since

$$\theta_i = \frac{\gamma_1 \hat{u}_i \hat{v}_i}{(m_1 \hat{v}_i + \hat{u}_i)^2} - \beta_1 \hat{u}_i,$$

by use of (3.1), we find that

$$\alpha_1 - \beta_1 \hat{u}_i = \frac{\gamma_1 \hat{v}_i}{m_1 \hat{v}_i + \hat{u}_i}, \quad \hat{v}_i = \frac{\hat{u}_i(\alpha_1 - \beta_1 \hat{u}_i)}{\gamma_1 - m_1(\alpha_1 - \beta_1 \hat{u}_i)}.$$

Therefore,

$$\theta_i = -[\beta_1 m_1 (\hat{u}_i)^2 - 2\beta_1(\alpha_1 m_1 - \gamma_1)\hat{u}_i + \alpha_1(\alpha_1 m_1 - \gamma_1)]/\gamma_1.$$

Set

$$f(\hat{u}_i) = \beta_1 m_1 (\hat{u}_i)^2 - 2\beta_1(\alpha_1 m_1 - \gamma_1)\hat{u}_i + \alpha_1(\alpha_1 m_1 - \gamma_1).$$

If $\alpha_1 m_1 > \gamma_1$, there exists a unique positive steady state $(\hat{u}_1, \hat{v}_1)$, and $(2\beta_1(\alpha_1 m_1 - \gamma_1))^2 - 4\beta_1 m_1 \alpha_1(\alpha_1 m_1 - \gamma_1) = -4\gamma_1 \beta_1^2(\alpha_1 m_1 - \gamma_1) < 0$. Thus, $f(\hat{u}_1) > 0$, that is, $\theta_1 < 0$.

If $\alpha_1 m_1 < \gamma_1$ and (2.4) hold, there exist two positive steady states $(\hat{u}_i, \hat{v}_i)(i = 2, 3)$, and $f = 0$ has a unique positive root u^*. Therefore, when $u^* < \hat{u}_2$, we conclude that $0 < f(\hat{u}_2) < f(\hat{u}_3)$, that is, $\theta_3 < \theta_2 < 0$. When $\hat{u}_2 < u^* < \hat{u}_3$, we have that $f(\hat{u}_2) < 0 < f(\hat{u}_3)$, that is, $\theta_3 < 0 < \theta_2$. When $u^* > \hat{u}_3$, we find that $f(\hat{u}_2) < f(\hat{u}_3) < 0$, that is, $\theta_2 > \theta_3 > 0$.

Appendix D. Global stability of the unique constant steady state $(\hat{u}_1, \hat{v}_1)$

We prove that the unique constant steady state $(\hat{u}_1, \hat{v}_1)$ is globally asymptotically stable given that the following condition holds

$$\alpha_1 m_1 > 2\gamma_1, \quad \gamma_2 > \alpha_2 m_1. \tag{D.1}$$

This condition is stronger than the one for local stability in Theorem 4.2. To prove the global stability, we first state a persistence property of the solution $(\hat{u}_1, \hat{v}_1)$, which implies that the prey and predator will always coexist at any time and any location of the habitat domain.

Proposition D.1. *Assume that $\alpha_1 m_1 > \gamma_1$. There exists a $t_0 \gg 1$ such that the solution $(u(x, t), v(x, t))$ of (3.1) and (3.2) satisfies*

$$(\alpha_1 m_1 - \gamma_1)/(m_1 \beta_1) - \varepsilon < u(x, t) < \alpha_1/\beta_1 + \varepsilon,$$
$$\alpha_2 m_2/\gamma_2 - \varepsilon < v(x, t) < \alpha_2(m_2 \beta_1 + \alpha_1)/(\beta_1 \gamma_2) + \varepsilon,$$

for all $x \in \bar{\Omega}$, $t \geq t_0$ *and* $0 < \varepsilon \ll 1$.

Proof. For $0 < \varepsilon \ll 1$, from (3.1) we can find that there exists a $t_0 \gg 1$ such that $u(x,t) < \alpha_1/\beta_1 + \varepsilon$ for all $x \in \bar{\Omega}$ and $t \geq t_0$ by the comparison principle for the parabolic equation. Hence, $v(x, t)$ is a lower solution of the following problem

$$\begin{cases} \dfrac{\partial z}{\partial t} - d\triangle z = \dfrac{\alpha_2(m_2 + \alpha_1/\beta_1 + \varepsilon) - \gamma_2 z}{m_2 + \alpha_1/\beta_1 + \varepsilon} z, \ \text{in } \Omega \times (t_0, \infty), \\ \partial_\eta z = 0, \ \text{on } \partial\Omega \times (t_0, \infty), \ z(x, t_0) = v(x, t_0), \ \text{on } \bar{\Omega}. \end{cases} \tag{D.2}$$

Let $v(t)$ be the unique positive solution of the problem

$$\begin{cases} w_t = \dfrac{\alpha_2(m_2 + \alpha_1/\beta_1 + \varepsilon) - \gamma_2 w}{m_2 + \alpha_1/\beta_1 + \varepsilon} w, \ \text{in } (t_0, \infty), \\ w(t_0) = \max_{\bar{\Omega}} v(x, t_0) > 0. \end{cases}$$

Then $v(t)$ is an upper solution of (D.2). As $\lim_{t\to\infty} v(t) = \alpha_2(m_2 + \alpha_1/\beta_1 + \varepsilon)/\gamma_2$, taking larger t_0 if necessary, we get from the comparison principle that $v(x,t) < v(t) + \varepsilon < \alpha_2(m_2\beta_1 + \alpha_1)/(\beta_1\gamma_2) + \varepsilon$ for all $x \in \bar{\Omega}$ and $t \geq t_0$.

Moreover, by (3.1) again, we have that $u(x, t)$ is an upper solution of

$$\begin{cases} \dfrac{\partial z}{\partial t} - \triangle z = (\alpha_1 - \beta_1 z - \gamma_1/m_1) z, \ \text{in } \Omega \times (t_0, \infty), \\ \partial_\eta z = 0, \ \text{on } \partial\Omega \times (t_0, \infty), \ z(x, t_0) = u(x, t_0), \ \text{on } \bar{\Omega}. \end{cases} \tag{D.3}$$

Let $u(t)$ be the unique positive solution of the problem

$$\begin{cases} w_t = (\alpha_1 - \beta_1 w - \gamma_1/m_1) w, \ \text{in } (t_0, \infty), \\ w(t_0) = \min_{\bar{\Omega}} u(x, t_0) > 0. \end{cases}$$

Then $u(t)$ is a lower solution of (D.3). As $\lim_{t\to\infty} u(t) = (\alpha_1 m_1 - \gamma_1)/(m_1\beta_1)$. Therefore, we deduce that for $x \in \bar{\Omega}$, $t \geq t_0$ and $0 < \varepsilon \ll 1$, $u(x,t) > u(t) - \varepsilon > (\alpha_1 m_1 - \gamma_1)/(m_1\beta_1) - \varepsilon$. Similarly to above argument, we can deduce that $v(x,t) > \alpha_2 m_2/\gamma_2 - \varepsilon$. The proof is completed. □

Now, we give the result of global stability of $(\hat{u}_1, \hat{v}_1)$ for system (3.1) and (3.2).

Theorem D.1. *Assume that the following condition (D.1) holds. Then* $(\hat{u}_1, \hat{v}_1)$ *is globally asymptotical stable for the system (3.1) and (3.2). In particular, this implies that (3.1) and (3.2) has no non-constant positive solutions.*

Proof. Let $(u(x, t), v(x, t))$ be the solution of (3.1) and (3.2). To prove our statement, we need to construct a Lyapunov functional. We define

$$\begin{aligned} W(u, v) &= \int \frac{u - \hat{u}_1}{u^2} \mathrm{d}u + \alpha \int \frac{v - \hat{v}_1}{v} \mathrm{d}v, \\ E(t) &= \int_\Omega W(u(x,t), v(x,t)) \mathrm{d}x, \end{aligned}$$

where α is a positive constant to be determined later.

By simple computation, it follows that

$$\begin{aligned} \frac{\mathrm{d}E(t)}{\mathrm{d}t} &= \int_\Omega \{W_u(u(x,t), v(x,t))u_t + W_v(u(x,t), v(x,t))v_t\} \mathrm{d}x \\ &= \int_\Omega \left\{ \frac{u - \hat{u}_1}{u^2} \Delta u + \alpha d \frac{v - \hat{v}_1}{v} \Delta v \right\} \mathrm{d}x \\ &\quad + \int_\Omega \left\{ \frac{u - \hat{u}_1}{u} \left(\alpha_1 - \beta_1 u - \frac{\gamma_1 v}{m_1 v + u} \right) + \alpha (v - \hat{v}_1) \left(\alpha_2 - \frac{\gamma_2 v}{m_2 + u} \right) \right\} \mathrm{d}x \\ &= -\int_\Omega \left\{ \frac{2\hat{u}_1 - u}{u^3} |\nabla u|^2 + \alpha d \frac{\hat{v}_1}{v^2} |\nabla v|^2 \right\} \mathrm{d}x \\ &\quad + \int_\Omega \left\{ \frac{u - \hat{u}_1}{u} \left(\beta_1 \hat{u}_1 + \frac{\gamma_1 \hat{v}_1}{m_1 \hat{v}_1 + \hat{u}_1} - \beta_1 u - \frac{\gamma_1 v}{m_1 v + u} \right) \right. \\ &\quad \left. + \alpha (v - \hat{v}_1) \left(\frac{\gamma_2 \hat{v}_1}{m_2 + \hat{u}_1} - \frac{\gamma_2 v}{m_2 + u} \right) \right\} \mathrm{d}x \\ &= -\int_\Omega \left\{ \frac{2\hat{u}_1 - u}{u^3} |\nabla u|^2 + \alpha d \frac{\hat{v}_1}{v^2} |\nabla v|^2 \right\} \mathrm{d}x \\ &\quad + \int_\Omega \left\{ (u - \hat{u}_1)^2 \left[-\frac{\beta_1}{u} + \frac{\gamma_1 \hat{v}_1}{u(m_1 \hat{v}_1 + \hat{u}_1)(m_1 v + u)} \right] - (v - \hat{v}_1)^2 \frac{\alpha \gamma_2}{m_2 + u} \right. \\ &\quad \left. + (u - \hat{u}_1)(v - \hat{v}_1) \left[\frac{\alpha \alpha_2}{m_2 + u} - \frac{\gamma_1 \hat{u}_1}{u(m_1 \hat{v}_1 + \hat{u}_1)(m_1 v + u)} \right] \right\} \mathrm{d}x \end{aligned}$$

Since $\gamma_2 > \alpha_2 m_1$, $\alpha_1 m_1 > 2\gamma_2$, and the Proposition D.1, we note that $2\hat{u}_1 - u > 0$ for $x \in \bar{\Omega}$, $t \gg 1$. By Proposition D.1 and $\alpha_1 m_1 > 2\gamma_1$, there exist positive constants α and t_0, such that for all $x \in \bar{\Omega}$ and $t \geq t_0$, we derive

$$\begin{aligned}&\alpha^2\alpha_2^2u^2(m_1\hat{v}_1+\hat{u}_1)^2(m_1v+u)^2+\gamma_1^2\hat{u}_1^2(m_2+u)^2\\&\quad+2\alpha u[2\gamma_1\gamma_2\hat{v}_1-2\beta_1\gamma_2(m_1\hat{v}_1+\hat{u}_1)(m_1v+u)-\alpha_2\gamma_1\hat{u}_1](m_1\hat{v}_1+\hat{u}_1)(m_1v+u)(m_2+u)\leq 0.\end{aligned}$$

Thus,

$$\begin{aligned}&(u-\hat{u}_1)^2\left[-\frac{\beta_1}{u}+\frac{\gamma_1\hat{v}_1}{u(m_1\hat{v}_1+\hat{u}_1)(m_1v+u)}\right]-(v-\hat{v}_1)^2\frac{\alpha\gamma_2}{m_2+u}\\&\quad+(u-\hat{u}_1)(v-\hat{v}_1)\left[\frac{\alpha\alpha_2}{m_2+u}-\frac{\gamma_1\hat{u}_1}{u(m_1\hat{v}_1+\hat{u}_1)(m_1v+u)}\right]\leq 0\end{aligned}$$

is satisfied. Then, $E'(t) < 0$ for $t > t_0$. Applying some standard arguments, together with the Proposition D.1 again, it follows that

$$(u(x,t),v(x,t)) \to (\hat{u}_1,\hat{v}_1) \text{ in } [L^\infty(\Omega)]^2.$$

This shows that $(\hat{u}_1,\hat{v}_1)$ attracts all solutions of (3.1) and (3.2). On the other hand, by Theorem 4.2, we see that $(\hat{u}_1,\hat{v}_1)$ is globally asymptotically stable. □

References

[1] Aly S, Kim I, Sheen D. Turing instability for a ratio-dependent predator–prey model with diffusion. Appl Math Comput 2011;217:7265–81.
[2] Arditi R, Ginzburg LR. Coupling in predator–prey dynamics: ratio-dependence. J Theor Biol 1989:311–26.
[3] Banerjee M. Self-replication of spatial patterns in a ratio-dependent predator–prey model. Math Comput Model 2010;51:44–52.
[4] Banerjee M, Abbas S. Existence and non-existence of spatial patterns in a ratio-dependent predator-prey model. Ecol Complex 2015;21:199–214.
[5] Banerjee M, Petrovskii S. Self-organised spatial patterns and chaos in a ratio-dependent predator–prey system. Theor Ecol 2011;4:37–53.
[6] Baurmann M, Gross T, Feudel U. Instabilities in spatially extended predator-prey systems: spatio-temporal patterns in the neighborhood of turing-hopf bifurcations. J Theor Biol 2007;245:220–9.
[7] Bishop MJ, Kelaher BP, Smith M, York PH, Booth DJ. Ratio-dependent response of a temperature australian estuarine system to sustained nitrogen loading. Oecologia 2006;149:701–8.
[8] Cantrell RS, Cosner C. Spatial ecology via reaction-diffusion equations. London: Wiley; 2003.
[9] Fasani S, Rinaldi S. Factors promoting or inhibiting turing instability in spatially extended prey–predator systems. Ecol Model 2011;222:3449–52.
[10] Gilad E, Shachak M, Meron E. Dynamics and spatial organization of plant communities in water limited systems. Theor Popul Biol 2007;72:214–30.
[11] Hanski I. The function response of predator: worries about scale. TREE 1991;6:141–2.
[12] Huffaker CB. Experimental studies predators: disperson factors and predator–prey oscillations. Hilgardia 1958;27:343–83.
[13] Klausmeier CA. Regular and irregular patterns in semiarid vegetation. Science 1999;284:1826–8.
[14] Kondo S, Miura T. Reaction-diffusion model as a framework for understanding biological pattern formation. Science 2010;329:1616–20.
[15] Levin SA. The problem of pattern and scale in ecology. Ecology 1992;73:1943–67.
[16] Liang Z, Pan H. Qualitative analysis of a ratio-dependent holling-tanner model. J Math Anal Appl 2007;34:954–64.
[17] Lin CS, Ni WM, Takagi I. Large amplitude stationary solutions to a chemotaxis systems. J Diff Equ 1988;72:1–27.
[18] Ling Z, Zhang L, Lin ZG. Turing pattern formation in a predator–prey system with cross diffusion. Appl Math Model 2015;38:5022–32.
[19] Lou Y, Ni WM. Diffusion, self-diffusion and cross-diffusion. J Diff Equ 1996;131:79–131.
[20] Luckinbill LS. Coexistence of laboratory populations of paramecium aurelia and its predator didinium nautum. Ecology 1973;54:1320–7.
[21] MacArthur RH, Wilson EO. The theory of island biogeography. Princeton: Princeton University Press; 1967.
[22] Malchow H. Spatio-temporal pattern formation in nonlinear nonequilibrium plankton dynamics. Proc R Soc Lond B 1993;251:103–9.
[23] Malchow H, Petrovskii SV, Venturino E. Spatiotemporal patterns in ecology and epidemiology: theory, models, and simulations. London: Chapman & Hall; 2008.
[24] Mandal PS, Banerjee M. Stochastic persistence and stability analysis of a modified holling-tanner model. M2AS 2013;36:1263–80.
[25] May RM. Stability and complexity in model ecosystems. Princeton: Princeton University Press; 2001.
[26] Medvinsky AB, Petrovskii SV, Tikhonova IA, Malchow H, Li BL. Spatiotemporal complexity of plankton and fish dynamics. SIAM Rev 2002;44:311–70.
[27] Meron E. Pattern-formation approach to modelling spatially extended ecosystems. Ecol Model 2012;234:70–82.
[28] Nindjin AF, Aziz-Alaoui MA, Cadivel M. Analysis of a predator–prey model with modified leslie–gower and holling-type II schemes with time delay. Nonlin Anal RWA 2006;7:1104–18.
[29] Okubo A. Diffusion and ecological problems: mathematical models. Berlin: Springer; 1980.
[30] Pang PYH, Wang M. Qualitative analysis of a ratio-dependent predator-prey system with diffusion. Proc Roy Soc Edinburgh 2003;133:919–42.
[31] Peng R, Yi FQ, Zhao XQ. Spatiotemporal patterns in a reaction-diffusion model with the degn–harrison reaction scheme. J Diff Eqn 2013;254:2465–98.
[32] Petrovskii SV, Malchow H. A minimal model of pattern formation in a prey–predator system. Math Comput Model 1999;29:49–63.
[33] Reeve JD. Predation and bark beetle dynamics. Oecologia 1997;112:48–54.
[34] Rietkerk M, Dekker SC, Ruiter PCD, Koppel JVD. Self-organized patchiness and catastrophic shifts in ecosystems. Science 2004;305:1926–9.
[35] Segel LA, Jackson JL. Dissipative structure: an explanation and an ecological example. J Theor Biol 1972;37:545–59.
[36] Sen M, Banerhee M, Morozov A. Bifurcation analysis of a ratio-dependent prey–predator model with the allee effect. Ecol Comp 2012;11:12–27.
[37] Seuront L. Fractals and multifractals in ecology and aquatic science. London: Chapman & Hall; 2009.
[38] Sherratt JA, Smith M. Periodic travelling waves in cyclic populations: field studies and reaction diffusion models. J R Soc Interface 2008;5:483–505.
[39] Shi JP. Semilinear neumann boundary value problems on a rectangle. Trans Amer Math Soc 2002;354:3117–54.
[40] Shi HB, Li WT, Lin G. Positive steady states of a diffusive predator–prey system with modified holling–tanner functional response. Nonlin Anal RWA 2010;11:3711–21.
[41] Shi HB, Ruan SG, Su Y, Zhang JF. Spatiotemporal dynamics of a diffusive leslie–gower predator–prey model with ratio-dependent functional response. Int J Bifurcat Chaos 2015;25:1530014.
[42] Shigesada N, Kawasaki K. Biological invasions: theory and practice. Oxford: Oxford University Press; 1997.
[43] Song YL, Zou XF. Spatiotemporal dynamics in a diffusive ratio-dependent predator-prey model near a hopf–turing bifurcation point. Comput Math Appl 2014;67:1978–97.
[44] Turchin P. Complex population dynamics. Princeton: Princeton University Press; 2003.
[45] Turing AM. The chemical basis of morphogenesis. Philos Trans R Soc Lond B 1952;237:37–72.
[46] Volpert AI, Volpert VA, Volpert VA. Traveling wave solutions of parabolic systems. Transl Math Monogr 1994. 140:American Mathematical Society, Providence RI.

[47] Wang MX. Stationary patterns for a prey–predator model with prey-dependent and ratio-dependent functional responses and diffusion. Physica D 2004;196:172–92.
[48] Wang W, Liu QX, Jin Z. Spatiotemporal complexity of a ratio-dependent predator–prey system. Phys Rev E 2007;75:051913.
[49] Wang L. Spatial pattern formation of a ratio-dependent predator–prey model. Chin Phys B 2010;9:09026.
[50] Wang J, Shi J, Wei JJ. Dynamics and pattern formation in a diffusive predator–prey system with strong allee effect in prey. J Diff Eqn 2011;251:1276–304.
[51] Yi FQ, Wei JJ, Shi J. Bifurcation and spatiotemporal patterns in a homogeneous diffusive predator–prey system. J Diff Eqn 2009;246:1944–77.
[52] Zhang L, Thygensen UH, Banerjee M. Size-dependent diffusion promotes the emergence of spatiotemporal patterns. Phys Rev E 2014;90:012904.
[53] Zuo WJ, Wei JJ. Stability and bifurcation in a ratio-dependent holling-III system with diffusion and delay. Nonlin Anal Model Control 2014;1:132–53.